

N66 30172

(ACCESSION NUMBER)

85

(PAGES)

CR-76103

(NASA CR OR TMX OR AD NUMBER)

(THRU)

(CODE)

(CATEGORY)

ELECTRICAL

## Digital Compensation Of The Thrust Vector Control System

PREPARED BY

SAMPLED - DATA CONTROL SYSTEMS GROUP

AUBURN UNIVERSITY

C. L. PHILLIPS, TECHNICAL DIRECTOR

GPO PRICE \$

CFSTI PRICE(S) \$

Hard copy (HC)

Microfiche (MF)

# 653 July 65

SECOND TECHNICAL REPORT

13 NOVEMBER, 1964 TO 28 MAY, 1965

CONTRACT - NAS8 - 11274

GEORGE C. MARSHALL SPACE FLIGHT CENTER

NATIONAL AERONAUTICS &amp; SPACE ADMINISTRATION

HUNTSVILLE, ALABAMA 35812

MAY 28, 1965

AUBURN RESEARCH FOUNDATION

AUBURN UNIVERSITY

AUBURN, ALABAMA

DIGITAL COMPENSATION OF THE THRUST  
VECTOR CONTROL SYSTEM

PREPARED BY

SAMPLED-DATA CONTROL SYSTEMS GROUP  
AUBURN UNIVERSITY

C. L. PHILLIPS, TECHNICAL DIRECTOR

SECOND TECHNICAL REPORT


13 NOVEMBER, 1964 TO 28 MAY, 1965

CONTRACT NAS8-11274


GEORGE C. MARSHALL SPACE FLIGHT CENTER  
NATIONAL AERONAUTICS AND SPACE ADMINISTRATION  
HUNTSVILLE, ALABAMA 35812

MAY 28, 1965

APPROVED BY

  
C. H. Weaver  
Head Professor  
Electrical Engineering

SUBMITTED BY

  
H. M. Summer  
Project Leader

## TABLE OF CONTENTS

LIST OF SYMBOLS.....	iv
LIST OF FIGURES.....	v
FORWARD.....	vii
SUMMARY.....	viii
PERSONNEL.....	ix
I. INTRODUCTION.....	1
II. FICTITIOUS SAMPLER AND FICTITIOUS HOLD METHOD.....	3
Derivation of Input-Output Expression of System Broken in $\beta_c$ Channel.....	3
Fictitious Sampler and Fictitious Hold Operating at a Multiple Rate of Basic Sampler...	4
Fictitious Sampler Operating at Basic Sampling Rate of System.....	6
Derivation of Approximate Transfer Function Using a Fictitious Sampler and Fictitious Ideal Hold.....	10
III. APPROXIMATE TRANSFER FUNCTION USING THE DESCRIBING FUNCTION ANALYSIS.....	16
Derivation of the Describing Function for the Sampler and Zero-Order Hold.....	16
The Describing Function of the Digital Compensator.....	18
The Nyquist Diagram of the System Using the Describing Function Approach.....	19

IV. CONCLUSIONS.....	24
REFERENCES.....	25
APPENDIX A.....	26
APPENDIX B.....	45
TABLE I.....	48

# LIST OF SYMBOLS

$D$	Digital compensator transfer function
$G_{1BN}$	Bending-modes transfer function in attitude channel
$G_{1R}$	Rigid body transfer function in attitude channel
$G_{2BN}$	Bending-modes transfer function in attitude rate channel
$G_{2R}$	Rigid body transfer function in attitude rate channel
$H_I$	Ideal hold transfer function
$H_O$	Zero-order hold transfer function
$R$	System input
$T$	Sampling period, seconds
$W_{ss}$	Control engine transfer function
$\beta_c$	Engine command signal
$\beta_e$	Continuous control engine deflection angle, degrees
$\phi$	Attitude error
$\dot{\phi}$	Attitude rate error
$\omega_s$	Sampling frequency, radians per second
$*$	Sampled signal

## LIST OF FIGURES

1. Sampled-data control system.....	49
2. System shown in Figure 1 broken at $\beta_e$ .....	50
3. System broken in $\beta_c$ channel with fictitious multirate sampler and hold at input terminal.....	51
4. Equivalent signal flow graph of multirate sampler.....	52
5. Composite signal flow graph of Figure 3 ( $N = 2$ ).....	53
6. Frequency spectrum of ideal sampler output.....	54
7. Gain and phase response for zero-order and polygonal hold versus $\omega$ .....	55
8. Nyquist diagrams of Figure 3 (with $N = 1$ ) for fictitious zero-order and polygonal holds.....	56
9. Gain characteristics of ideal filter.....	57
10. Open-loop sampled system.....	57
11. Sampled system with an unsampled input.....	58
12. System shown in Figure 3 with fictitious sampler and ideal hold inserted at the input terminal.....	58
13. System shown in Figure 1 redrawn.....	59
14. Sampled system including bending modes.....	60
15. Input and output wave of the sampler and zero-order hold.....	61

16.	Nyquist diagram for system shown in Fig. 14 opened in $\phi$ channel (no bending modes).....	62
17.	Nyquist diagram for system shown in Fig. 14 opened in $\dot{\phi}$ channel (no bending modes).....	63
18.	Nyquist diagram for system shown in Fig. 14 opened in $\beta_c$ channel (no bending modes).....	64
19.	Nyquist diagram for system shown in Fig. 14 opened in $\phi$ channel (four bending modes).....	65
20.	Nyquist diagram for system shown in Fig. 14 opened in $\dot{\phi}$ channel (four bending modes).....	66
21.	Nyquist diagram for system shown in Fig. 14 opened in $\beta_c$ channel (four bending modes).....	67
22.	Nyquist diagram for system shown in Fig. 14 opened in $\phi$ channel using single precision z-transform methods (four bending modes).....	68

## FORWARD

This report is a technical summary of the progress made since the November 13, 1964 technical report by the Electrical Engineering Department, Auburn University, toward fulfillment of Contract No. NAS8-11274 granted to Auburn Research Foundation, Auburn, Alabama. The contract was awarded May 28, 1964, by the George C. Marshall Space Flight Center, National Aeronautics and Space Administration, Huntsville, Alabama.



## SUMMARY

Open-loop pulsed transfer functions of the simplified thrust vector control system for a Saturn-type vehicle with an unsampled input are derived by the fictitious sampler and fictitious hold method and by the describing function method. Both methods are approximate with accuracy depending on the low-pass nature of the system. Typical examples of both methods are given.

## PERSONNEL

The following named staff members of Auburn University have actively participated on this project.

- C. H. Weaver - Head Professor of Electrical Engineering
- H. M. Summer - Professor Electrical Engineering
- G. T. Nichols - Associate Professor of Electrical Engineering
- C. L. Phillips - Associate Professor Electrical Engineering
- C. L. Rogers - Assistant Professor of Electrical Engineering
- R. E. Littleton - Instructor of Electrical Engineering
- J. S. Boland - Graduate Assistant in Electrical Engineering
- D. W. Kelly - Graduate Assistant in Electrical Engineering

## DIGITAL COMPENSATION OF THE THRUST VECTOR CONTROL SYSTEM

### I. INTRODUCTION

A complete analysis of the system shown in Figure 1 requires the determination of the gain and phase margins in each of the three channels. These margins may be determined analytically by breaking the system in each of the three channels, obtaining the open-loop transfer function of the system for each channel respectively, and investigating the Nyquist diagram of each of these transfer functions about the minus one point. An open-loop transfer function can readily be obtained if the input signal is sampled before passing through a continuous-data element. An example is the system shown in Figure 1 broken at the point  $\phi$ . A open-loop transfer function can not be written, however, if the input signal is acted upon by a continuous-data element in the system before being sampled. An example is the system shown in Figure 1 broken at the point  $\beta_e$  or at the point  $\dot{\phi}$ .

This report is concerned with obtaining a Nyquist diagram for the system shown in Figure 1 broken at  $\beta_e$ . The two methods described are the fictitious sampler and fictitious hold method and the describing function method. Both methods are approximate and depend on the low-pass nature of the system. The two methods and the limitations of each are presented in the following sections of this report.

Appendix A gives some basic sampled-data control system theory and has been included to provide a common ground for the reading of this report.

## II. FICTITIOUS SAMPLER AND FICTITIOUS HOLD METHOD

J. S. Boland

This chapter is concerned with the derivation of an approximate transfer function of the system shown in Figure 1 broken in the  $\beta_c$  channel.

### Derivation of Input-Output Expression of System Broken in $\beta_c$ Channel

In order to determine the gain and phase margins of the system shown in Figure 1 broken at  $\beta_e$ , the open-loop transfer function must be obtained at this point. If the system is broken as shown in Figure 2, the sampled output,  $X_o^*$ , is given by

$$X_o^*(s) = \left[ X_i G_2 W_{ss}(s) \right]^* + \left[ X_i G_1(s) \right]^* \cdot \left[ H_o W_{ss}(s) \right]^* \quad (1)$$

Equation (1), however, is not a true transfer function since the input,  $X_i$ , cannot be factored out of the output expression. If both sides of (1) are divided by  $X_i^*(s)$ , the resulting transfer function is dependent on the input and is therefore not a true transfer function. In general, if the input to a discrete system is acted upon by a continuous-data element before being sampled, it cannot be factored out of the resulting output expression and therefore no transfer function can be written.

### Fictitious Sampler and Fictitious Hold Operating at a Multiple Rate of Basic Sampler

Since a transfer function for a discrete system cannot be written unless the input is sampled, one method of obtaining an approximate transfer function is to insert a fictitious sampler and fictitious hold at the input terminal as shown in Figure 3. The fictitious sampler, however, introduces an infinite number of harmonic components that are not present in the original system. The effects of these harmonics will now be investigated.

First, the possibility of operating the fictitious sampler at a much higher rate than the rate of the basic sampler was investigated. The higher the sampling frequency of the fictitious sampler, the less effect it has on system performance. Theoretically as the sampling frequency approaches infinity, the effects of the fictitious sampler and hold become completely negligible.

The fictitious sampler can be represented by a flow graph as shown in Figure 4 if its sampling rate is an integral multiple,  $N$ , of the basic sampling rate of the sampler in the  $\phi$  channel. Figure 5 is the composite signal flow graph representing the system shown in Figure 3 illustrating the case of the sampling rate of the fictitious sampler being twice that of the digital sampler. By using Mason's gain formula<sup>1</sup> the pulsed output,  $X_O^*(s)$ , can be expressed as

$$\begin{aligned}
X_o^*(s) = X_i^*(s) & \left( \left[ W_{ss} G_2 H_o \right]^* (s) + \left[ G_1 H_o \right]^* (s) \left[ W_{ss} H_o \right]^* (s) \right) \\
& + \left[ X_i(s) e^{sT/2} \right]^* \left( \left[ W_{ss} G_2 H_o e^{-sT/2} \right]^* (s) + \left[ G_1 H_o e^{-sT/2} \right]^* (s) \left[ W_{ss} H_o \right]^* (s) \right)
\end{aligned} \quad (2)$$

No transfer function can be obtained from (2) since  $X_i(s)$  cannot be factored out of the second term. This is true because

$$\mathcal{Z} \left[ e^{sT/2} X_i(s) \right] \neq z^{1/2} X_i(z) \quad (3)$$

The generalized form of (2) expressed in modified z-transform form is<sup>2</sup>

$$\begin{aligned}
X_o(z) = X_i(z) & \left( \left[ W_{ss} G_2 H_o \right](z) + \left[ G_1 H_o \right](z) \left[ W_{ss} H_o \right](z) \right) \\
& + z \sum_{P=1}^{N-1} X_i(z, P/N) \left( \left[ W_{ss} G_2 H_o \right](z, 1-P/N) \right. \\
& \left. + \left[ G_1 H_o \right](z, 1-P/N) \left[ W_{ss} H_o \right](z) \right)
\end{aligned} \quad (4)$$

where

$$\mathcal{Z} \left[ e^{PTs/N} E(s) \right] = z E(z, P/N) \quad 0 < P/N \leq 1$$

and

$$\mathcal{Z} \left[ e^{-PTs/N} E(s) \right] = E(z, 1-P/N) \quad 0 < P/N \leq 1$$

The results of (2), (3), and (4) show that if the rate of the fictitious sampler is not identical to the basic sampling rate of the system, no transfer function can be written.

#### Fictitious Sampler Operating at Basic Sampling Rate of System

Since, as shown in the above section, a transfer function cannot be obtained for the system broken in the  $\beta_c$  channel unless the signal is sampled in this channel at the same rate as the sampler in the  $\phi$  channel, the effects of adding a fictitious sampler and hold in the  $\beta_c$  channel and then compensating analytically for their effects on the system was investigated.

If the continuous input to the fictitious sampler is  $E(s)$ , the sampled output is given by

$$E^*(s) = \frac{1}{T} \sum_{n=-\infty}^{\infty} E(s + jn\omega_s) + \frac{e(o^+)}{2} \quad (5)$$

The  $\frac{e(o^+)}{2}$  term in (5) is included to account for the effect of the sampler when the input signal has a jump discontinuity,  $e(o^+)$ , at  $t = 0$ . For the system shown in Figure 3 (with  $N = 1$ ), the  $\frac{e(o^+)}{2}$  term



is zero. If the highest input frequency of the input signal,  $e(t)$ , to the sampler is  $\omega_c$ , the frequency spectrum of the sampler output is as shown in Figure 6. For some input frequency  $\omega < \omega_c$  the output magnitude and phase in Figure 3 will be the combined effect of the fundamental plus all the harmonic frequency components of the sampler output.

In selecting the fictitious hold to be used, one of the desired characteristics is a high attenuation of the higher frequency harmonics generated by the sampler. The zero-order and polygonal holds were considered with transfer functions as given below.

$$H_o = \frac{1 - e^{-sT}}{s}$$

$$H_p = \frac{e^{Ts}(1 - e^{-Ts})^2}{Ts^2}$$

(6)

The polygonal hold is not physically realizable since it requires a predictor, but this causes no concern here since it is introduced fictitiously and used only for analytical analysis. The gain and phase plots for varying  $\omega$  for the two holds are as shown in Figure 7. It was felt that the polygonal hold would give better results since it introduces no phase shift and attenuates the higher frequency components considerably more than the zero-order hold.

In addition to the attenuation introduced by the hold, the low-pass nature of the system will also attenuate the harmonic components of the output of the sampler. Considering only six bending modes, the highest frequency component that must be considered is approximately  $\omega_s/4$ , or 6.25 hz. The predominant reflected frequency for this input frequency is 25 hz - 6.25 hz or 18.75 hz. The polygonal hold attenuates this reflected frequency by 20.9 db in addition to the attenuation introduced by the system. For input frequencies less than 6.25 hz, the attenuation of the first reflected frequency by the polygonal hold is much greater.

If the fictitious sampler shown in Figure 3 is operating at the same rate as the sampler in the  $\phi$  channel, the open-loop approximate transfer function for the system broken in the  $\beta_c$  channel is

$$\frac{X_o(z)}{X_i(z)} = \left[ HG_1(z) \right] \left[ H_o W_{ss}(z) \right] + G_2 HW_{ss}(z) \quad (7)$$

The transfer functions shown in the block diagrams of Figures 1, 2, and 3 are defined as follows:

$$\begin{aligned} G_1(s) &= \frac{-0.94068468}{s^2 - 0.029727836} \\ G_2(s) &= \frac{-0.94068468 s}{s^2 - 0.029727836} \\ W_{ss}(s) &= \frac{625}{s^2 + 25s + 625} \end{aligned} \quad (8)$$

The constants of these transfer functions were taken from a set of typical data at forty seconds flight time for a Saturn V vehicle.

Curve A of Figure 8 is the Nyquist diagram of the continuous system shown in Figure 3 with both samplers and the fictitious hold removed and is included for comparison purposes. Curve B is the compensated Nyquist diagram of the sampled system with a fictitious zero-order hold in the  $\beta_c$  channel. The compensated Nyquist diagram is the diagram of (7) with the db attenuation and phase lag introduced by the fictitious zero-order hold on the fundamental frequency added back into the diagram. Curve C is the compensated Nyquist of the sampled system with a fictitious polygonal hold in the  $\beta_c$  channel. Curve C, however, coincided with Curve A out to approximately 8 hz and could not be plotted as a separate curve. The frequency responses of both the zero-order hold and polygonal hold are shown in Figure 7.

As shown in Figure 8, the fictitious polygonal hold gives more accurate results than the fictitious zero-order hold. This was expected, however, since the polygonal hold attenuates the higher frequency components introduced by the fictitious sampler more than the zero-order hold. It should be pointed out that the sampled-system Nyquist should not correlate exactly with the continuous Nyquist because of the higher frequency harmonics introduced by the sampler in the  $\phi$  channel. Most of the effects of these higher harmonics, however, are filtered out by the low-pass nature of the system for input frequencies less than  $\omega_s/4$ .

It is concluded that both the fictitious zero-order hold and the fictitious polygonal hold will yield accurate results at frequencies less than  $\omega_s/4$  with the polygonal hold yielding the most accurate results up to approximately 8 or 9 hz.

#### Derivation of Approximate Transfer Function Using a Fictitious Sampler and Fictitious Ideal Hold

In the previous section of this chapter an approximate transfer function was obtained by inserting a fictitious sampler and fictitious hold at the input terminal. The best fictitious hold is one that completely filters out the harmonics generated by the fictitious sampler. The polygonal hold used in the previous section is the best hold found that can be expressed analytically. This hold was seen to yield good results for the low-pass system shown in Figure 1.

The effects of the harmonics generated by the fictitious sampler can be completely eliminated by using a fictitious ideal filter with characteristics as shown in Figure 9. The ideal filter can be represented by

$$H_I(j\omega) = A(\omega)e^{j\theta(\omega)} \quad (9)$$

where

$$\begin{aligned} A(\omega) &= T & |\omega| &\leq |\omega_s/2| \\ A(\omega) &= 0 & |\omega| &> |\omega_s/2| \end{aligned} \quad (10)$$

and  $\theta(\omega) = 0$ , giving no phase shift through the filter.

The system of Figure 10 will be used to illustrate the development of a transfer function. The sampled output for Figure 10 is given by

$$C^*(s) = R^*(s) H_I G^*(s) \quad (11)$$

The open-loop transfer function of the system shown in Figure 10 is

$$\frac{C^*(s)}{R^*(s)} = H_I G^*(s) = \frac{1}{T} \sum_{n=-\infty}^{+\infty} H_I G(s + jn\omega_s) \quad (12)$$

Expanding (12),

$$\begin{aligned} \frac{C^*(s)}{R^*(s)} = \frac{1}{T} & \left[ H_I G(j\omega) + H_I G(j\omega - j\omega_s) + H_I G(j\omega + j\omega_s) \right. \\ & \left. + H_I G(j\omega - 2j\omega_s) + H_I G(j\omega + 2j\omega_s) + \dots \right] \end{aligned} \quad (13)$$

If the input frequency,  $\omega$ , is less than  $\omega_s/2$ , all of the terms in (13) with the exception of the first term will be zero, since, as shown in Figure 9, the ideal hold completely attenuates all frequencies greater in magnitude than  $\omega_s/2$ . Therefore (13) reduces to

$$\frac{C^*(j\omega)}{R^*(j\omega)} = \frac{1}{T} H_I G(j\omega) = \frac{1}{T} G_I(j\omega) G(j\omega) \quad (14)$$

But from Figure 9,  $H_I(j\omega) = T$  for  $|\omega|$  less than  $|\omega_s/2|$ . Therefore (13) becomes

$$\frac{C^*(j\omega)}{R^*(j\omega)} = \frac{1}{T} (T) G(j\omega)$$

or

$$\frac{C^*(j\omega)}{R^*(j\omega)} = G(j\omega) \quad (15)$$

The output of the ideal hold in Figure 10 is  $R(s)$ , since  $H_I(s)$  exactly reconstructs the sampled input. Therefore the continuous output in Figure 10 is

$$C(j\omega) = G(j\omega) R(j\omega)$$

or

$$\frac{C(j\omega)}{R(j\omega)} = G(j\omega) \quad (16)$$

Equations (15) and (16) show that for input frequencies less than  $\omega_s/2$ , there is no effect from the insertion of the sampler and ideal hold into the system.

The results shown in (15) and (16) are very important when analyzing systems with inputs that are not sampled before passing through a continuous element. The sampled output of Figure 11 is

$$C^*(s) = \left[ GR^*(s) \right] \left[ H_O W_{ss}^*(s) \right] \quad (17)$$

No transfer function can be written since the input cannot be factored out of the output expression in (17). By inserting a fictitious sampler and ideal hold at the input terminal as shown in Figure 12 and using the results of (15) and (16), a transfer function can be obtained and is given by

$$\frac{C^*(j\omega)}{R^*(j\omega)} = G(j\omega) \left[ \frac{1}{T} \sum_{n=-\infty}^{+\infty} H_O W_{ss}(j\omega + jn\omega_s) \right] \quad (18)$$

Equation (18) is valid only for input frequencies less than  $\omega_s/2$ . For  $0 \leq \omega \leq \omega_s/2$ , (18) gives an exact Nyquist diagram for the open-loop system shown in Figure 11.

If the open-loop system shown in Figure 11 is closed, however, (18) does not give an accurate Nyquist diagram for the closed-loop system about the minus one point. The reason for the inaccuracy is the harmonic components generated by the sampler being fed back into  $G(s)$ . The effects of the harmonics were not considered in the open-

loop system. If the system is low-pass, however, these harmonic components are negligible, thereby allowing the negative of (18) to be investigated about the minus one point to determine the gain and phase margins of the closed-loop system.

The ideal hold method of analysis can be applied to the system shown in Figure 2 with transfer functions as defined by (6) and (8). The open-loop transfer function, O.L.T.F., obtained by the fictitious sampler and fictitious ideal hold method of analysis presented above is

$$\text{O.L.T.F.} = G_2 W_{ss}(s) + G_1(s) \left[ \frac{1}{T} \sum_{n=-\infty}^{+\infty} H_o W_{ss}(s + jn\omega_s) \right] \quad (19)$$

When the loop is closed at  $\beta_e$ , the system shown in Figure 1 can be redrawn as shown in Figure 13. The closed-loop transfer function can now be expressed as

$$\frac{X_o}{X_i} = \frac{\text{O.L.T.F.}}{1 - \text{O.L.T.F.}}$$

or

$$\frac{X_o}{X_i} = \frac{\text{O.L.T.F.}}{1 + (-\text{O.L.T.F.})} \quad (20)$$



The Nyquist of the negative open-loop transfer function was then obtained by using the digital computer program shown in Appendix B. This Nyquist differed from the continuous Nyquist shown in curve A of Figure 8 by only .05 db and .3 degrees at  $\omega = \omega_s / 2$  and therefore could not be plotted as a separate curve. This indicates that the effects of harmonics generated by the sampler can be considered negligible for the low-pass system given by (8).

Although the ideal hold method of analysis agrees very closely with the continuous system, it is believed to be more accurate than the continuous system since the effects of the higher harmonics generated by the sampler in the forward loop are considered. However, more work must be done in this area with systems that are not as low-pass as the system described by (8) to determine the validity of this statement.

### III. APPROXIMATE TRANSFER FUNCTION USING THE DESCRIBING FUNCTION ANALYSIS

R. E. Littleton

Figure 14 is a block diagram of the thrust-vector control system including the bending modes. An open-loop transfer function can be written when the system is broken in the  $\phi$  channel only. However, an open-loop transfer function is needed for each channel. An approximate method is given below which will allow a transfer function to be written for the other channels. The method uses describing-function techniques.

#### Derivation of the Describing Function for the Sampler and Zero-Order Hold

Figure 15 is a graph of the input and output to the sampler and zero-order hold where the input is  $\phi_i(t) = \sin(\omega t + \theta)$ . Then

$$\phi_i^*(t) = \sum_{n=0}^{\infty} \sin(\omega nT + \theta) \delta(t - nT) \quad (21)$$

and

$$\phi_o(t) = \sum_{n=0}^{\infty} \sin(\omega nT + \theta) \left( u(t - nT) - u\left[t - (n + 1)T\right] \right) \quad (22)$$

The Fourier series for  $\phi_o(t)$  can be used to find the magnitude of its fundamental frequency. The Fourier coefficients,  $C_k$ , where

$$\phi_o(t) = \sum_{k=-\infty}^{\infty} C_k e^{j \frac{k 2 \pi t}{L}} \quad (23)$$

and where  $L$  is the total period of the output wave, are

$$C_k = \frac{1}{\pi} \sum_{n=0}^{q-1} \sin(n\omega T + \Theta) \sin\left(\frac{k\pi T}{L}\right) e^{-jk\pi(2n+1)T/2} \quad (24)$$

$q$  is defined as  $Tq = L$ , and is the smallest possible integer. The magnitude of the  $k^{\text{th}}$  harmonic of the output is  $2|C_k|$ .

The plots of the magnitude and phase lag of the fundamental frequency of  $\phi_o(t)$  are given in Figure 7. The plots were found to be the same as that for the transfer function of the zero-order hold,

$$H_o(j\omega) = \frac{1 - e^{-j\omega T}}{j\omega} \quad (25)$$

with the exception of  $\omega = \omega_s/2$ . At  $\omega = \omega_s/2$

$$2|C_1| = \frac{4}{\pi} |\sin\Theta|. \quad (26)$$

This occurs because, at an input frequency of  $\omega_s/2$ , the output fundamental is composed of two terms. The additional term is due to the reflected frequency and the sum of the two terms is phase sensitive. The transfer function of the zero-order hold is therefore used for its describing function.

The describing function is good only for frequencies less than  $\omega_s/2$ . This is true since, for an input frequency greater than  $\omega_s/2$ , a subharmonic frequency is generated at a frequency less than  $\omega_s/2$ . This subharmonic cannot be ignored.

#### The Describing Function of the Digital Compensator

According to J. M. Salzer,<sup>3</sup> the substitution  $z = e^{sT} \Big|_{s=j\omega} = e^{j\omega T}$  may be used for the digital program of the digital computer since the program only holds, sums and multiples. Therefore the transfer function of the digital compensator used in Chapter IV of the first technical report

$$D(z) = \frac{(z - 0.99)}{z - 0.90} \quad (27)$$

becomes

$$D(j\omega) = \frac{e^{j\omega T} - 0.99}{e^{j\omega T} - 0.90} \quad (28)$$

for the frequency analysis.  $D(j\omega)$  is the describing function for the digital compensator.

The same  $D(z)$  may be realized using a zero-order hold and continuous network but the frequency response would depend on the type network used, since the same  $z$ -transform may be obtained with different types of networks.

The Nyquist Diagram of the System Using the Describing Function Approach

The following equations were used for the transfer functions of the system shown in Figure 14.

$$H_o(s) = \frac{25(1 - e^{-Ts})}{s} \quad (29)$$

$$D(s) = \frac{(e^{Ts} - 0.99)}{(e^{Ts} - 0.90)} \quad (30)$$

$$W_{ss}(s) = \frac{625}{s^2 + 25s + 625} \quad (31)$$

$$GIR(s) = \frac{-0.94068468}{s^2 - 0.02972784} \quad (32)$$

$$GIB1(s) = \frac{0.0065323138(s^2 + 498.59362)}{s + 0.064905305s + 42.126986} \quad (33)$$

$$GIB2(s) = \frac{-0.0040378959(s^2 + 485.48033)}{s^2 + 0.12013450s + 144.32299} \quad (34)$$

$$GIB3(s) = \frac{-0.0053896739(s^2 + 470.36052)}{s^2 + 0.1837817s + 337.76255} \quad (35)$$

$$GIB4(s) = \frac{0.0058368238(s^2 + 469.03256)}{s^2 + 0.22481237s + 505.40603} \quad (36)$$

$$G2R(s) = \frac{-0.94068468s}{s - 0.02972784} \quad (37)$$

$$G2B1(s) = \frac{0.0065323138s(s^2 + 498.59362)}{s^2 + 0.064905305s + 42.126986} \quad (38)$$

$$G2B2(s) = \frac{-0.0040378959s(s + 485.48033)}{s^2 + 0.12013450s + 144.32299} \quad (39)$$

$$G2B3(s) = \frac{-0.0053896739s(s + 470.36052)}{s^2 + 0.18378317s + 337.76255} \quad (40)$$

$$G2B4(s) = \frac{0.0058368238s(s^2 + 469.03256)}{s^2 + 0.22481237s + 505.40603} \quad (41)$$

$$GIB5(s) = GIB6(s) = G2B5(s) = G2B6(s) = 0 \quad (42)$$

The equations for the bending-mode effects were obtained from the data furnished by the Astronics Laboratory, Marshall Space Flight Center at 40 seconds of flight time.

The Nyquist diagrams of the system broken in the different channels using the describing-function approach are given in Figures 16, 17, 18, 19, 20 and 21. The plots are shifted  $180^\circ$  in order to use the -1 point or 0 db at 180 degrees for determining the stability of the system.

The equations used to obtain the open-loop response broken in the different channels are:

$$\phi \text{ open-loop} = \frac{DH_O W_{SS} (G1R + G1B1 + G1B2 + G1B3 + G1B4)}{1 - W_{SS} (G2R + G2B1 + G2B2 + G2B3 + G2B4)} (j\omega) \quad (43)$$

$$\phi \text{ open-loop} = \frac{W_{SS} (G2R + G2B1 + G2B2 + G2B3 + G2B4)}{1 - W_{SS} (G1R + G1B1 + G1B2 + G1B3 + G1B4) DH_O} (j\omega) \quad (44)$$

$$\beta_c \text{ open-loop} = W_{SS} \left[ (G2R + G2B1 + G2B2 + G2B3 + G2B4) + (G1R + G1B1 + G1B2 + G1B3 + G1B4) DH_O \right] (j\omega) \quad (45)$$

Figures 16, 17 and 18 are with no bending modes and Figures 19, 20 and 21 are with 4 bending modes.

An attempt was made to check the results of  $\phi$  open-loop using the describing function with that of  $\phi$  open-loop using the z-transform Nyquist diagram since a transfer function can be written for this case. Trouble was encountered carrying enough significant figures in the z-transform computer program. See Figure 22. Thus,

$$G^*(s) = \frac{1}{T} \sum_{n=-\infty}^{\infty} G(s + jn\omega_s) + g(0^+) \gamma_2 \quad (46)$$

was used instead.<sup>4</sup> For a low-pass system, good results are obtained using only a few terms of (47). Then,

(47)

$$\phi \text{ open-loop} = \frac{1}{T} \sum_{n=-\infty}^{\infty} \frac{DH_o(G1R + G1B1 + G1B2 + G1B3 + G1B4)}{1 - (G2R + G2B1 + G2B2 + G2B3 + G2B4)} (j\omega + jn\omega_s)$$

The results of (47) are shown in Figure 19 for two cases, first when (47) was approximated varying  $n$  through  $\pm 2$  and when  $n$  was varied through  $\pm 10$ . The two cases were practically identical so this was considered as the correct Nyquist diagram. The difference in the two cases was in the second and third significant figures. Appendix B is a sample program of the digital program used to make these calculations. Also, as can be seen from the same figure, the describing function Nyquist diagram obtained is nearly the same as that when using (47). Thus, the describing function approach should give excellent results. See Table 1. The poles of  $\phi$  open-loop are

$$s = \sum_{n=-\infty}^{\infty} -2.63 + jn\omega_s$$

$$s_1 = 0.0$$

$$s_2 = -0.9527$$

$$s_3 = 0.0306$$



$$s_4 = 1.283 - j6.104$$

$$s_5 = 1.283 + j6.104$$

$$s_6 = - 0.5337 - j12.48$$

$$s_7 = - 0.5337 + j12.48$$

$$s_8 = - 0.1477 - j22.61$$

$$s_9 = - 0.1477 + j22.61$$

$$s_{10} = - 11.69 - j21.67$$

$$s_{11} = 11.69 + j21.67$$

$$s_{12} = - 0.3320 - j18.75$$

$$s_{13} = - 0.3320 + j18.75$$

The system is unstable with the bending modes included since there are three poles of the open-loop transfer function in the right-half  $s$ -plane,  $P = 3$  and  $N = 1$ . Therefore,  $z = P - N = 2$ .

#### IV. CONCLUSIONS

The fictitious sampler and fictitious ideal hold method of analysis gives an exact Nyquist for the open-loop system shown in Figure 2. When the loop is closed, however, investigation of the open-loop Nyquist about the minus one point leads to inaccurate results due to the higher harmonics generated by the sampler in the  $\phi$  loop being fed back. If the system is low-pass, however, the effects of these harmonics will be negligible. Since the system shown in Figure 2 and described by (8) is low-pass, the fictitious sampler and hold method of analysis gives good results.

As can be seen from Figure 19, the describing function technique gives good results for frequencies less than 10 cps. The results of the Nyquist diagram using single precision on the computer for z-transform methods were not satisfactory and were inconclusive. This can be seen by comparing Figures 19 and 22. However, good results are obtainable for a low pass system by the z-transform method if the transfer function is approximated by a few terms of the infinite-series representation as given in (47). The digital computer program can be in single precision. The describing-function technique shows that the system is unstable with and without the bending mode effects with no compensation. The system is stable with the compensator,  $D(z)$ , in (27), for the rigid body case and unstable when including the bending mode effects. Therefore, some other compensator is needed to stabilize the system for both cases.

#### REFERENCES

1. S. J. Mason, "Feedback theory - some properties of signal flow graphs," Proc. I.R.E., vol 41, pp 1144-1156; September, 1953.
2. B. C. Kuo, Analysis and Synthesis of Sampled-Data Control Systems, Prentice-Hall, Inc., Englewood Cliffs, N. J., pp. 353-364; 1963.
3. J. M. Salzer, "Frequency Analysis of Digital Computers Operating in Real Time," Proc. I.R.E., vol. 42, No. 2; pp. 457-466, 1954.
4. B. C. Kuo, op.cit. p. 34.
5. Pierre and Kolb, "Concerning the Laplace transform of sampled signals," I.E.E.E. Trans. on Automatic Control, vol. AC-9, pp. 191-192; April, 1964.

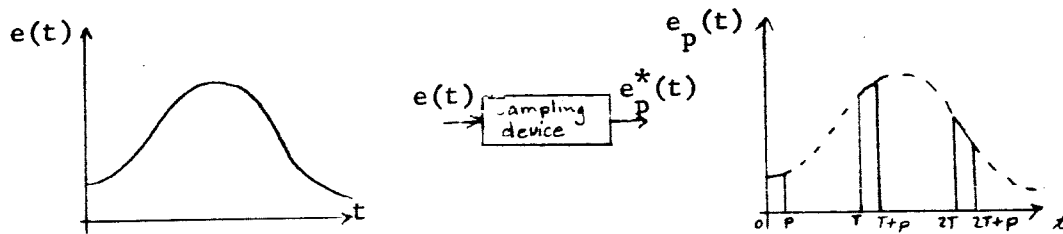
## APPENDIX A

### SAMPLED-DATA CONTROL SYSTEMS-BASIC THEORY

C. L. Phillips

#### Sampling Operation

The sampling operation is defined as shown:



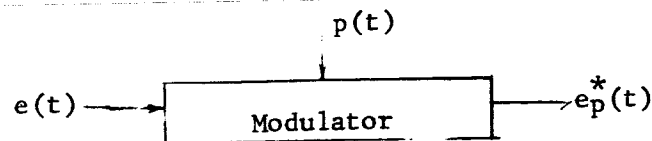
For

$$nT \leq t \leq nT + p, \quad n = 0, 1, 2, \dots, \quad e_p^*(t) = e(t),$$

and for

$$nT + p \leq t \leq (n + 1)T, \quad e_p^*(t) = 0.$$

The sampling operation can be considered as a modulation process,



where

$$p(t) = \sum_{n=0}^{\infty} \left[ u(t - nT) - u(t - nT - p) \right]$$

Then

$$e_p^*(t) = e(t)p(t)$$

Assumption 1: The pulse width,  $p$ , is small compared to the dominant time constants of the system. Then

$$e_p^*(t) \approx e_1^*(t) = pe(0)\delta(t) + pe(T)\delta(t-T) + pe(2T)\delta(t-2T) + \dots$$

Assumption 2: Each sampler is followed by a data-hold device. (This assumption is justified in the section on data holds.) Then the output of the sampler, which is referred to as an ideal sampler, is

$$\frac{e(t)}{\text{ideal sampler}} \longrightarrow e^*(t)$$

$$e^*(t) = e(0)\delta(t) + e(T)\delta(t-T) + \dots = \sum_{n=0}^{\infty} e(nT)\delta(t-nT)$$

The Laplace transform of  $e^*(t)$  is

$$E^*(s) = \mathcal{L} [e^*(t)] = \sum_{n=0}^{\infty} e(nT)e^{-nTs}$$

$E^*(s)$  can be expressed in a different manner. Let

$$\delta_T(t) = \sum_{n=-\infty}^{\infty} \delta(t - nT)$$

and suppose

$$e(t) = 0 \quad \text{for} \quad t < 0.$$

Then

$$e^*(t) = e(t)\delta_T(t)$$

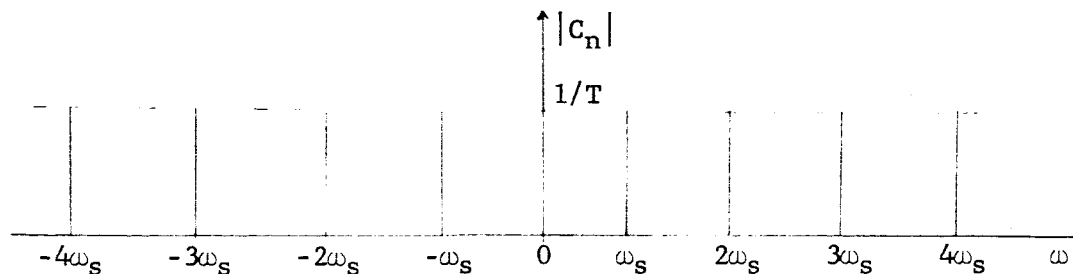
By Fourier analysis

$$\delta_T(t) = \sum_{n=-\infty}^{\infty} \delta(t-nT) = \sum_{n=-\infty}^{\infty} c_n e^{jn\omega_s t}, \quad \omega_s = \frac{2\pi}{T}$$

Now

$$\begin{aligned} c_n &= \frac{1}{T} \int_{-T/2}^{T/2} \delta_T(t) e^{-jn\omega_s t} dt = \frac{1}{T} \int_{-T/2}^{T/2} \delta(t) e^{-jn\omega_s t} dt \\ &= \frac{1}{T} \int_{-\epsilon/2}^{\epsilon/2} \delta(t) dt = \frac{1}{T} \end{aligned}$$

The frequency spectrum of  $\delta_T(t)$  is



Then

$$e^*(t) = e(t)\delta_T(t) = \frac{1}{T} \sum_{n=-\infty}^{\infty} e(t)e^{jn\omega_s t}$$

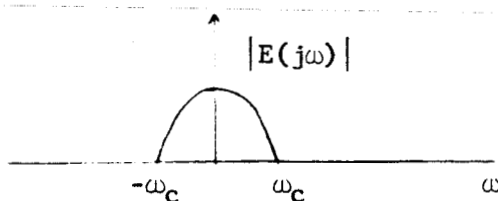
Thus

$$E^*(s) = \frac{1}{T} \sum_{n=-\infty}^{\infty} E(s + jn\omega_s) + \frac{e(0^+)}{2}$$

The term  $e(0^+)/2$  does not appear in the derivation, because  $\delta(t)$  was assumed to occur with its weight equally distributed about the origin.

If  $\delta(t^+)$  were used, where the weight of  $\delta(t^+)$  occurs at  $t = 0^+$ , this term would appear. This term should be present. For a derivation, see Pierre and Kolb, Reference 5.

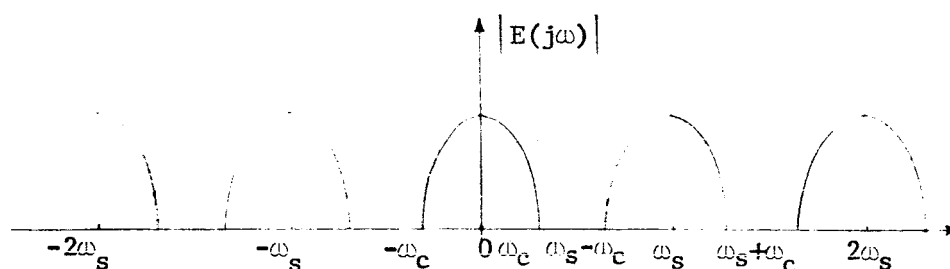
If the signal  $e(t)$  has the frequency spectrum



then, from

$$E^*(s) = \sum_{n=-\infty}^{\infty} E(s + jn\omega_s) + \frac{e(0^+)}{2}$$

$E^*(s)$  has the frequency spectrum



From this spectrum it is seen that the original signal can be recovered by an ideal low-pass filter if

$$\omega_s - \omega_c > \omega_c$$

or

$$\omega_s > 2\omega_c$$

This illustrates Shannan's sampling theorem, which states that if a signal contains no frequency higher than  $\omega_c$  radians per second, it is completely characterized by the values of the signal measured at instants of time separated by  $T = \frac{1}{2}(2\pi/\omega_c)$  second.

Still another expression for  $E^*(s)$  can be obtained by complex convolution. Since

$$e^*(t) = e(t)\delta_T(t)$$

then

$$\begin{aligned} E^*(s) &= E(s) \otimes \Delta_T(s) = \frac{1}{2\pi j} \int_{C-j\infty}^{C+j\infty} E(\zeta) \Delta_T(s - \zeta) d\zeta \\ &= \frac{1}{2\pi j} \int_{C-j\infty}^{C+j\infty} \Delta_T(\zeta) E(s - \zeta) d\zeta \end{aligned}$$



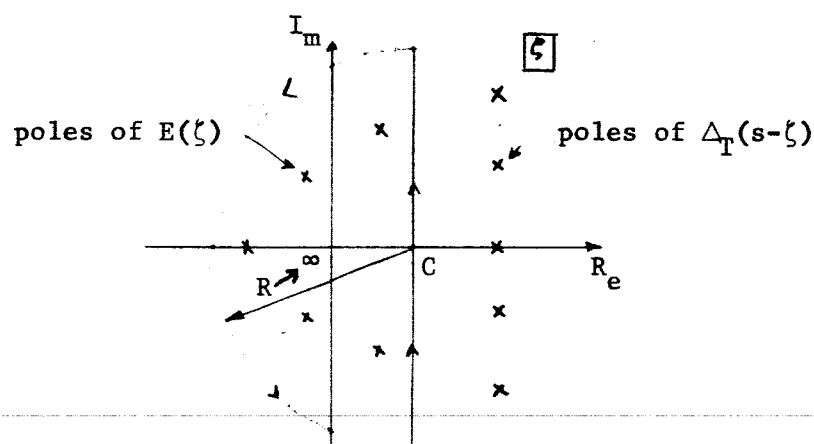
Now

$$\Delta_T(s) = \mathcal{L} [\delta_T(t)] = 1 + e^{-Ts} + e^{-2Ts} + \dots = \frac{1}{1 - e^{-Ts}}, \quad |e^{-Ts}| < 1$$

Using the first integral above for  $E^*(s)$ ,

$$E^*(s) = \frac{1}{2\pi j} \int_{C-j\infty}^{C+j\infty} E(\zeta) \frac{1}{1 - e^{-T(s-\zeta)}} d\zeta$$

the conditions on  $C$  are such that the poles of the two functions in the  $\zeta$ -plane are as shown.



The integral can be expressed as the integral around the closed path minus the integral around the infinite arc. If

$$\lim_{\zeta \rightarrow \infty} \zeta E(\zeta) = 0$$

$$\zeta \rightarrow \infty$$

then the integral around the infinite arc is zero, and

$$E^*(s) = \sum_{\substack{\text{residues of } E(\zeta)\Delta_T(s-\zeta) \\ \text{at poles} \\ \text{of } E(\zeta)}}$$

Using

$$E^*(s) = \frac{1}{2\pi j} \int_{C-j\infty}^{C+j\infty} \Delta_T(\zeta) E(s-\zeta) d\zeta$$

The poles of  $\Delta_T(\zeta)$  now fall within the closed path. Then

$$E^*(s) = \sum_{\substack{\text{residues of } \Delta_T(\zeta)E(s-\zeta) \\ \text{at poles} \\ \text{of } \Delta_T(\zeta)}}$$

The poles of  $\Delta_T(\zeta)$  occur at  $\zeta = \pm jn\omega_s$ ,  $n = \text{all integers}$ , and

$$E^*(s) = \frac{1}{T} \sum_{n=-\infty}^{\infty} E(s + jn\omega_s)$$

If

$$\lim_{\zeta \rightarrow \infty} \zeta E(\zeta) = e(0^+) \neq 0,$$

the term  $e(0^+)/2$  must be added to the equation for  $E^*(s)$ . See the above reference to Pierre and Kolb for the proof.

#### Properties of $E^*(s)$

- 1)  $E^*(s)$  is a periodic function with a period  $j\omega_s$ .

Proof:

$$E^*(s) = \sum_{n=0}^{\infty} e(nT) e^{-nTs}$$

$$E^*(s + jn\omega_s) = \sum_{n=0}^{\infty} e(nT) e^{-nTs} e^{-jnm\omega_s T} \quad m = \text{integer}$$

Now

$$e^{-jnm\omega_s T} = e^{-jnm\omega_s 2\pi/\omega_s} = e^{-jnm2\pi} = 1$$

Thus

$$E^*(s + jn\omega_s) = \sum_{n=0}^{\infty} e(nT) e^{-nTs} = E^*(s)$$

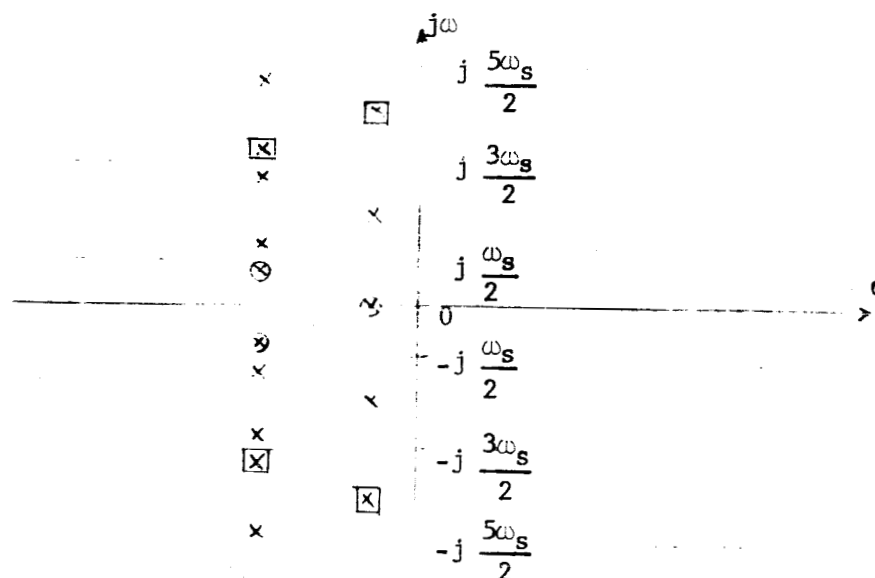
2) If  $E(s)$  has a pole at  $s = s_1$ , then,  $E^*(s)$  must have poles at  $s = s_1 + jn\omega_s$  ( $m = \text{all integers from } -\infty \text{ to } +\infty$ ).

Proof: If  $e(0^+) = 0$ ,

$$E^*(s) = \frac{1}{T} \sum_{n=-\infty}^{\infty} E(s + jn\omega_s) = \frac{1}{T} \left[ \dots + E(s - jn\omega_s) + E(s) + E(s + jn\omega_s) + \dots \right]$$

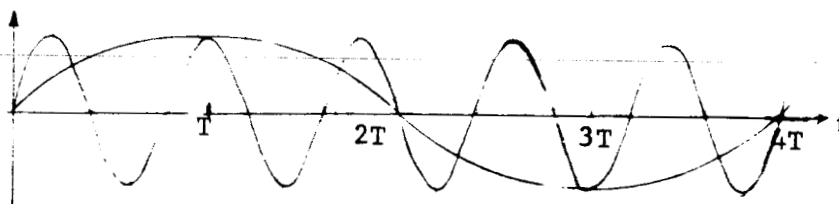
A result of this property is shown in the s-plane diagram. Assume that the circled poles shown are the poles of  $E(s)$ . Then  $E^*(s)$  has the poles shown. The poles of  $E^*(s)$  occur in periodic strips. The strip centered about the real axis is referred to as the primary strip, and all other strips are referred to as complementary strips. If the

original poles of  $E(s)$  had been



those shown boxed, the pole distribution of  $E^*(s)$  would not change.

This is shown by the figure below. Note that even though the frequencies of the two sine waves are different, the sampled output waves are the same.



### Data Holds

The output signal of a sampling device is not in useful form, but must be recovered by a data hold. Let

$$e_n(t) = e(t) \quad \text{for} \quad nT \leq t \leq (n+1)T$$

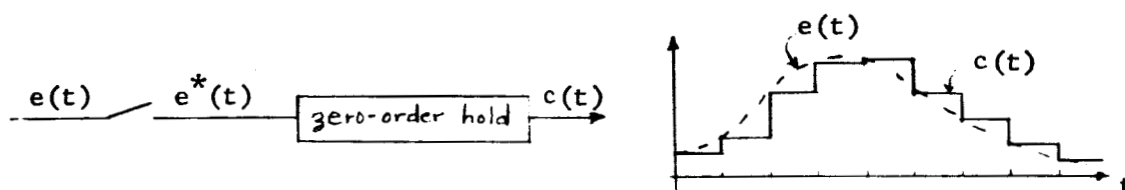
where  $e(t)$  is the signal prior to sampling. Now, by Taylor's series expansion

$$e_n(t) = e(nT) + e'(nT)(t-nT) + \frac{e''(nT)}{2!} (t-nT)^2 + \dots$$

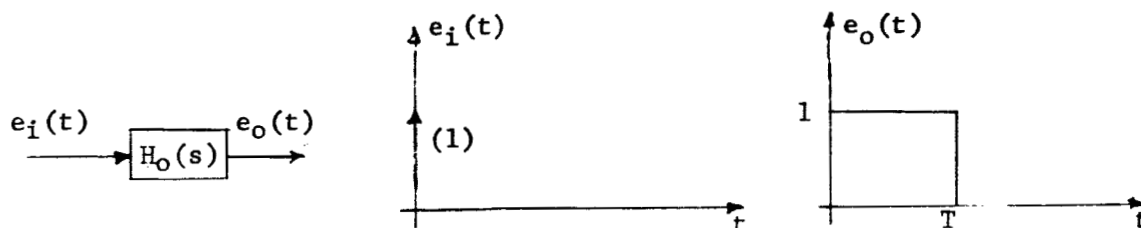
To rebuild the signal exactly, all of the terms of the expansion must be used. Practically, only the first term is used in a zero-order hold, the first two terms in a first-order hold, etc. For the zero order hold,

$$e_n(t) = e(nT) \quad nT \leq t \leq (n+1)T$$

An example is given in the figure below.



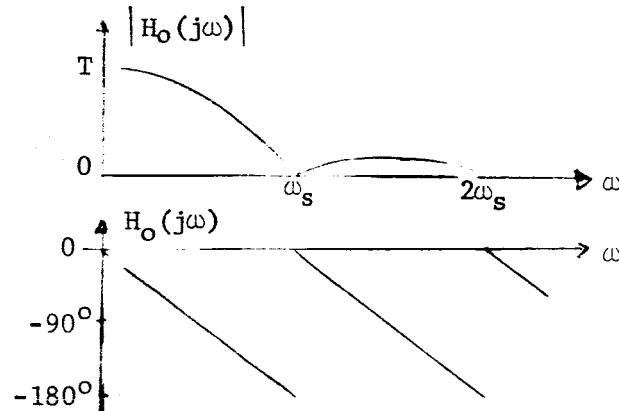
To determine the transfer function of a zero-order hold, for a unit impulse input, the output must be as shown. Let  $H_0(s)$  be the transfer



function of the zero-order hold. Then

$$E_O(s) = H_O(s)E_i(s) = H_O(s) = \frac{1 - e^{-Ts}}{s}$$

The frequency response of a zero-order hold is as shown.

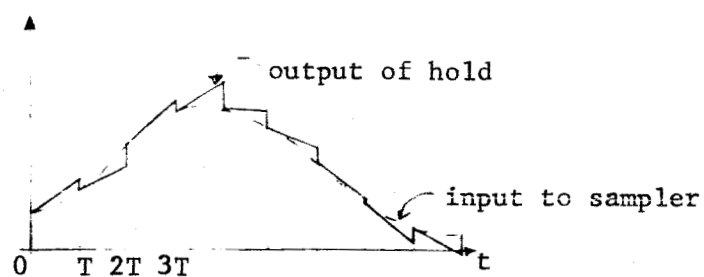


As stated originally, the width of the pulses,  $p$ , may be omitted if the sampling device is followed by a hold. In the physical system, the hold does not have the transfer function given, since, in the physical system, the input pulses are of finite height. However, the output of the physical hold is identical with the output of  $H_O$ . Thus, in either case, the correct signal appears at the output of the data hold.

For the first-order hold, the value  $e'(nT)$  is not known. It is normally approximated by

$$e'(nT) = \frac{e(nT) - e[(n-1)T]}{T}$$

An example using the first-order hold is given below.



### z-transform

As has been shown,  $E^*(s)$  is a transcendental function. The complex variable  $s$  appears only in the form  $e^{sT}$ . If the substitution is made

$$z = e^{sT}$$

then

$$E(z) = \mathcal{L} \left[ e^*(t) \right]_{s = \frac{1}{T} \ln z}$$

and  $E(z)$  is a rational fraction in  $z$ .  $E(z)$  is termed the  $z$ -transform of  $e(t)$ , or the  $z$ -transform of  $E(s)$ . Since

$$E^*(s) = \sum_{n=0}^{\infty} e(nT) e^{-nTs}$$

then

$$E(z) = \sum_{n=0}^{\infty} e(nT) z^{-n}$$

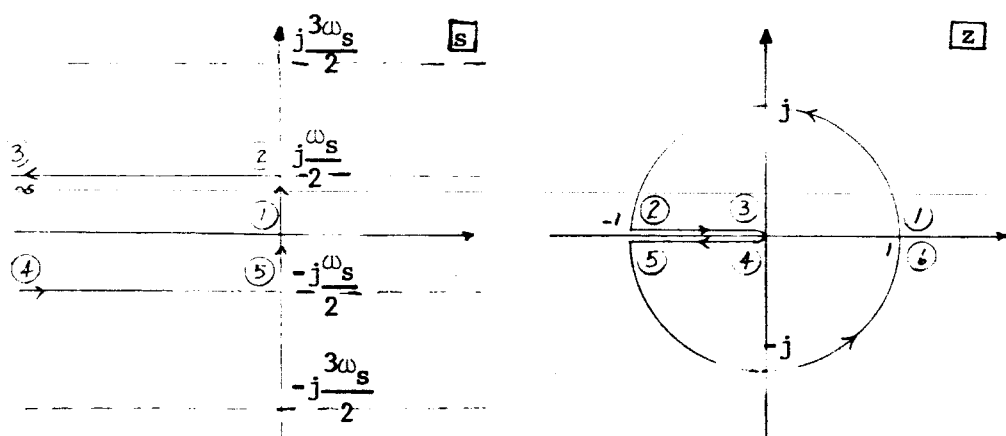
Also, since

$$E^*(s) = \sum_{\text{at poles of } E(\zeta)} \text{residues of } E(\zeta) \frac{1}{1 - e^{-T(s-\zeta)}}$$

then

$$E(z) = \sum_{\text{at poles of } E(\zeta)} \text{residues of } E(\zeta) \frac{1}{1 - e^{T\zeta} z^{-1}}$$

Consider the z-transform in terms of transforming from the s-plane to the z-plane. It is seen that the primary strip in the left half of the s-plane transforms into the interior of the unit circle in the

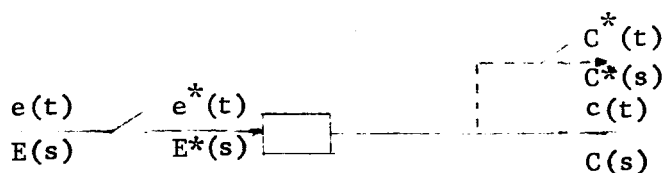


z-plane. Also, it is seen that each complementary strip in the left half of the s-plane transforms into the interior of the unit circle in the z-plane.



### System Analysis

Consider the open-loop system



Now

$$C(s) = G(s)E^*(s)$$

$$C^*(s) = \frac{1}{T} \sum_{n=-\infty}^{\infty} C(s+jn\omega_s) = \frac{1}{T} \sum_{n=-\infty}^{\infty} G(s+jn\omega_s)E^*(s+jn\omega_s)$$

But

$$E^*(s+jn\omega_s) = E^*(s)$$

Thus

$$C^*(s) = E^*(s) \frac{1}{T} \sum_{n=-\infty}^{\infty} G(s+jn\omega_s) = E^*(s)G^*(s)$$

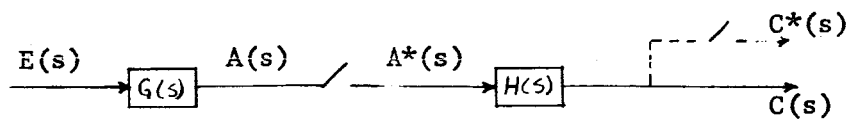
Or

$$\frac{C^*(s)}{E^*(s)} = G^*(s)$$

Or

$$\frac{C(z)}{E(z)} = G(z)$$

Also consider



Now

$$C(s) = H(s)A^*(s)$$

$$C^*(s) = H^*(s)A^*(s)$$

Also

$$A(s) = G(s)E(s)$$

$$A^*(s) = \frac{1}{T} \sum_{n=-\infty}^{\infty} G(s + jn\omega_s) E(s + jn\omega_s)$$

Now

$$\frac{1}{T} \sum_{n=-\infty}^{\infty} G(s + jn\omega_s) E(s + jn\omega_s) \neq \frac{1}{T} \sum_{n=-\infty}^{\infty} G(s + jn\omega_s) \frac{1}{T} \sum_{n=-\infty}^{\infty} E(s + jn\omega_s)$$

Thus

$$A^*(s) = (GE)^*(s) \neq G^*(s)E^*(s)$$

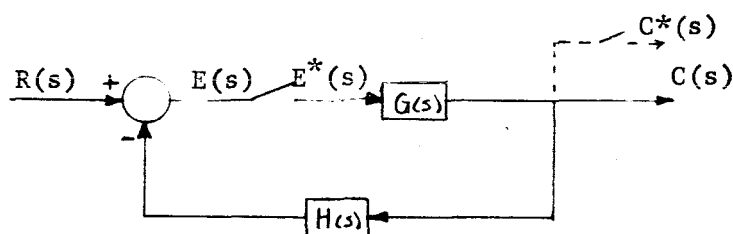
and

$$C^*(s) = H^*(s)(GE)^*(s)$$

$$C(z) = H(z)GE(z)$$

For this system, a transfer function independent of  $E(s)$  cannot be written. In general, if the input signal is not sampled prior to being applied to a continuous-data transfer function, a transfer function for the system cannot be written.

Consider the closed-loop system



Now

$$E(s) = R(s) - H(s)C(s) = R(s) - G(s)H(s)E^*(s)$$

$$E^*(s) = R^*(s) - (GH)^*(s)E^*(s)$$

Or

$$E^*(s) = \frac{R^*(s)}{1 + (GH)^*(s)}$$

Thus

$$C(s) = G(s)E^*(s) = \frac{G(s)R^*(s)}{1 + (GH)^*(s)}$$

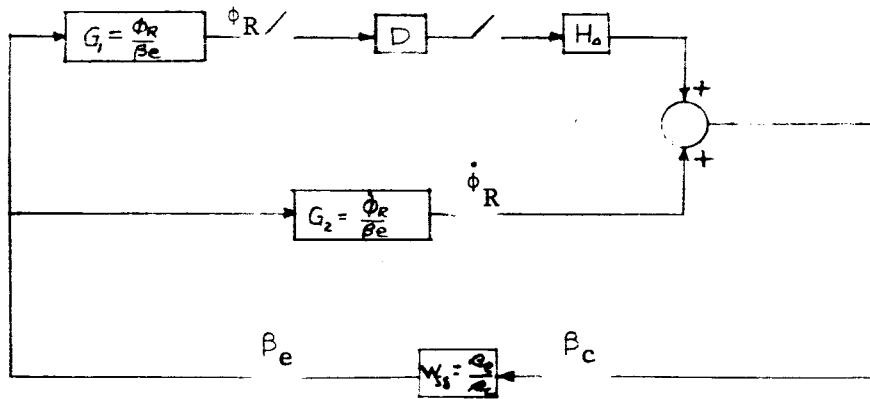
and

$$\frac{C^*(s)}{R^*(s)} = \frac{G^*(s)}{1 + (GH)^*(s)}$$

Or

$$\frac{C(z)}{R(z)} = \frac{G(z)}{1 + GH(z)}$$

Consider the rigid body system for a Saturn-type vehicle with the  $\gamma$  channel omitted.



D represents a digital compensator and  $H_0$  a zero-order hold. If the system is opened at  $\phi_R$ , with an input  $E_i(s)$  and an output  $E_o(s)$ , then

$$\beta_e = W_{ss} G_2 \beta_e + W_{ss} H_0 D^* E_i^*$$

Or

$$\beta_e = \frac{W_{ss} H_0 D^* E_i^*}{1 - W_{ss} G_2}$$

$$E_o = G_1 \beta_e = \frac{W_{ss} G_1 H_o}{1 - W_{ss} G_2} D^* E_i^*$$

Or

$$E_o^* = \left( \frac{G_1 W_{ss} H_o}{1 - W_{ss} G_2} \right)^* D^* E_i^*$$

Thus

$$\frac{E_o(z)}{E_i(z)} = \left( \frac{G_1 W_{ss} H_o}{1 - W_{ss} G_2} \right) (z) D(z)$$

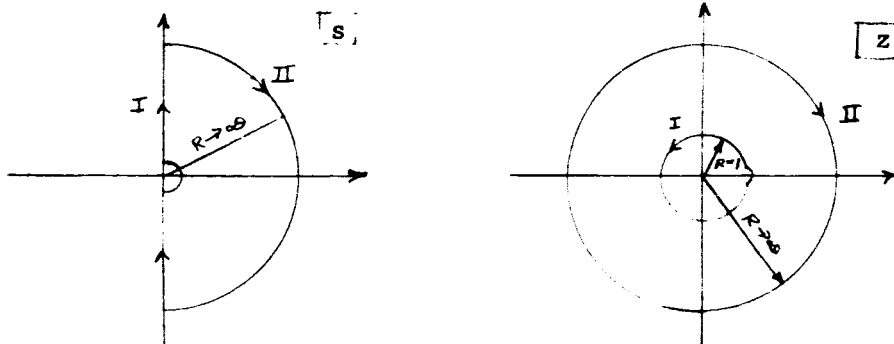
If the system is opened at  $\beta_e$ ,

$$E_o = W_{ss} \beta_e = W_{ss} G_2 E_i + W_{ss} H_o D^* (G_1 E_i)^*$$

For this case, no transfer function is possible.

### Nyquist Criterion

The Nyquist criterion is applicable to the z-plane if the correct path is used. The Nyquist path is the s-plane transforms into the path shown in the z-plane through the transformation  $z = e^{sT}$ .

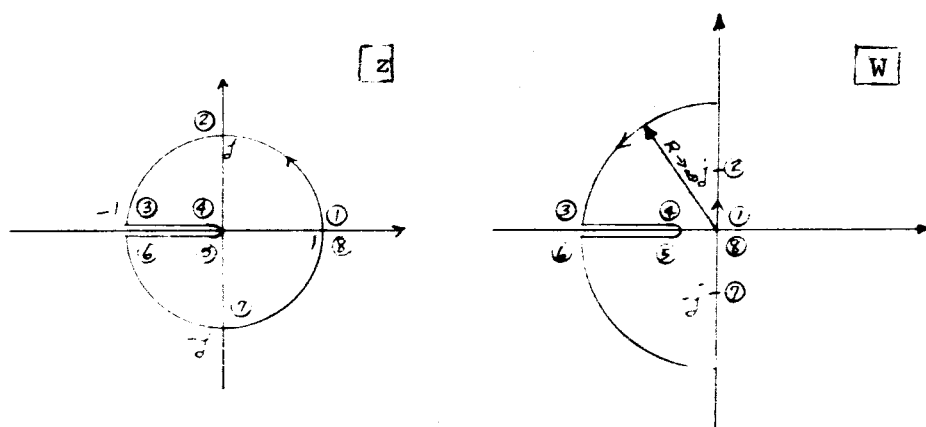


For cases that only the  $j\omega$  axis is required in the s-plane, only the unit circle is required in the z-plane. Note that the left halfplane of the s-plane transforms into the interior of the unit circle in the z-plane.

For certain applications, it may be more convenient to work in a plane that has the same properties of the s-plane with respect to stability. The w-plane has these properties. The transformation

$$z = \frac{1 + w}{1 - w}$$

The unit circle in the z-plane transforms as shown. The imaginary



axis in the w-plane is the boundary between the stable region for poles (the left halfplane) and the unstable region (the right halfplane).

## APPENDIX B

## Digital Computer Program for Infinite Series Expansion of Sampled-Data System

```

C *****
C FREQ. DUM. - INF. SERIES METHOD *****
C *****
1 10 FORMAT(5(X,E15.8))
2 20 FORMAT(7X,92HFREQ(HERTZ)          FREQ(RADIANS)      MAGNITUDE
3 1      MAGNITUDE IN DB      ANGLE IN DEG,/)
4 30 FORMAT(1P-1)
5 PRINT 20
6 PIC = 3.1415926
7 T = 0.04
8 COMPLEX S,FALLP,C(5)
9 COMPLEX G1R,G1B1,G1B2,G1B3,G1B4,G2R,G2B1,G2B2,G2B3,G2B4,
10 1WWW,HUL,GIG
11 DEM = PIF/(T*180.0)
12 K = 1
13 DEG = 0.0
14 WS = (2.0*PIE)/T
15 1 IF (DEG.GT.5.0) GO TO 11
16 IF (DEG.GT.0.1) GO TO 13
17 DEG = DEG + 0.01
18 GO TO 12
19 13 DEG = DEG + 0.1
20 GO TO 12
21 11 DEG = DEG + 0.1
22 12 W = DEG*DEM
23 S = CMPLX(0.0,W)
24 C(1) = (0.0,0.0)

```

Digital Computer Program  
(Continued)

```

33      DO 34 J=1,21
34      N = - 11 + J
35      XN = N
36      W1 = W + XN*WS
37      S = CMPLX(0.0,W1)
38      G1B1=(0.65323138E-02)*(S**2 + (498.59362,0.0))/
39      1(S**2 + (C.64905305E-01)*S + (42.126986,0.0))
40      G1B2= - (C.40378959E-02)*
41      1(S**2 + (485.48033,0.0))/(S**2 + 0.1201345*S + (144.32299,0.0))
42      G1B3 = -(0.53896739E-02)*(S**2 + (470.36052,0.0))/
43      1(S**2 + 0.18378317*S + (337.76255,0.0))
44      G1B4 = (C.58368238E-02)*(S**2 + (469.03256,0.0))/
45      1(S**2 + 0.22481237*S + (505.40603,0.0))
46      G2B1 = S*G1B1
47      G2B2 = S*G1B2
48      G2B3 = S*G1B3
49      G2B4 = S*G1B4
50      G1R = -(0.94068468)/(S**2 - (0.02972784,0.0))
51      G2R = S*G1R
52      HUL = (1.00)*(1.0,0.0) - CEXP(-T*S))/(S)
53      WWW= (625.0)/(S**2 + 25.0*S + (625.0,0.0))
54      DIG = (1.000)*(CEXP(T*S) - (0.99,0.0))/(CEXP(T*S) - (0.90,0.0))
55      C(2) = HCLDIG*WWW*(G1R + G1B1 + G1B2 + G1B3 + G1B4)/
56      1 ((1.0,0.0) - WWW*(G2R + G2B1 + G2B2 + G2B3 + G2B4))
57      34 C(1) = C(1) + C(2)*25.0
58      HELP = C(K)
59      XREAL = REAL(HELP)
60
61

```



Digital Computer Program  
(Continued)

```

62 XIMAG = AIMAG(HELP)
63 XMAG = Sqrt(XREAL**2+XIMAG**2)
64 ANGLE = ATAN(XIMAG/XREAL)
65 IF(XREAL.EQ.0.0) IF(XIMAG) 3,4,5
70 IF(XREAL.GT.0.0) GO TO 6
73 IF(XREAL.LT.0.0) IF(XIMAG) 2,2,8
76 ANGLE = ANGLE+ PIE
77 GO TO 6
100 2 ANGLE = ANGLE - PIE
101 GO TO 6
102 3 ANGLE = -PIE/2.0
103 4 GO TO 6
104 5 ANGLE = PIE/2.0
105 6 ANGLE = ANGLE*180.0/PIE
106 FREQ = W/(2.0*PIE)
107 DB = 20.C*ALOG10(XMAG)
110 PRINT 10 ,FREQ,W,XMAG,DB,ANGLE
111 IF(W-78.80) 1,1,7
112 7 K = K+1
113 IF (K.EQ.2) STOP
116 PRINT 30
117 GO TO 9
120 END

```

TABLE 1

Comparison of the Describing Function and Equation (47)  
When Broken in  $\phi$  Channel (See Fig. 19)

Freq. hz	Describing Function		Equation (47) ( $n = \frac{1}{2}$ )		Equation (47) ( $n = \frac{1}{10}$ )	
	Mag. dB.	Angle deg.	Mag. db.	Angle deg.	Mag. db.	Angle deg.
0.07	-7.8	112	-7.8	112	-7.8	112
0.76	-16.8	56	-16.8	56	-16.8	56
1.25	-21.2	129	-21.2	129	-21.2	129
3.06	-27.0	-46	-27.0	-46	-27.0	-46
5.00	-50.4	-148	-50.4	-148	-50.4	-148
7.50	-61.0	162	-61.0	165	-61.1	165
8.00	-62.3	157	-62.7	159	-62.8	159
8.50	-63.7	149	-64.3	154	-64.5	154
9.00	-65.1	144	-65.9	150	-65.9	150
9.50	-66.4	138	-67.6	147	-67.8	147
10.5	-67.7	132	-69.3	144	-69.5	144
11.0	-70.0	122	-72.9	145	-73.3	147
12.5	-73.4	108	-77.4	176	-77.4	180

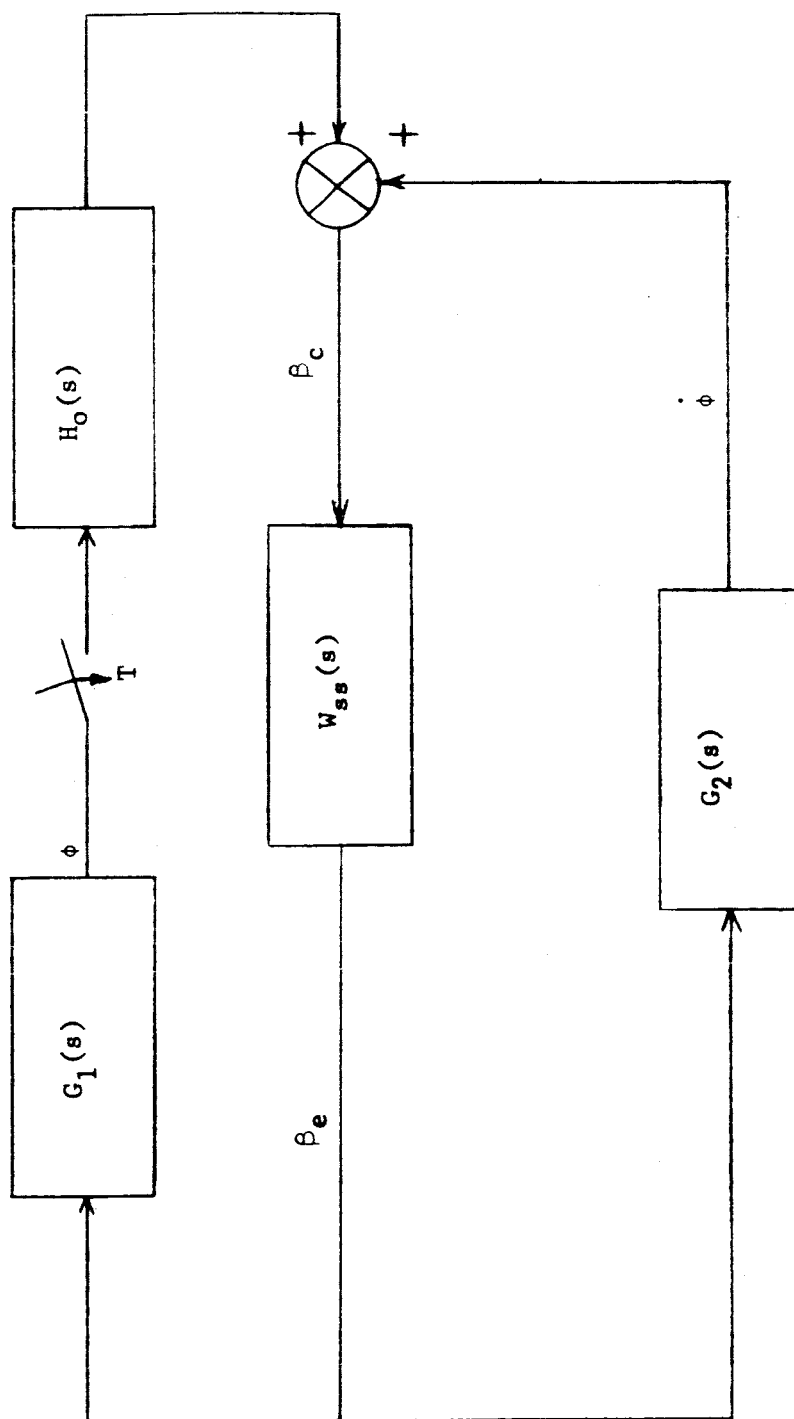


Fig. 1--Sampled-data control system

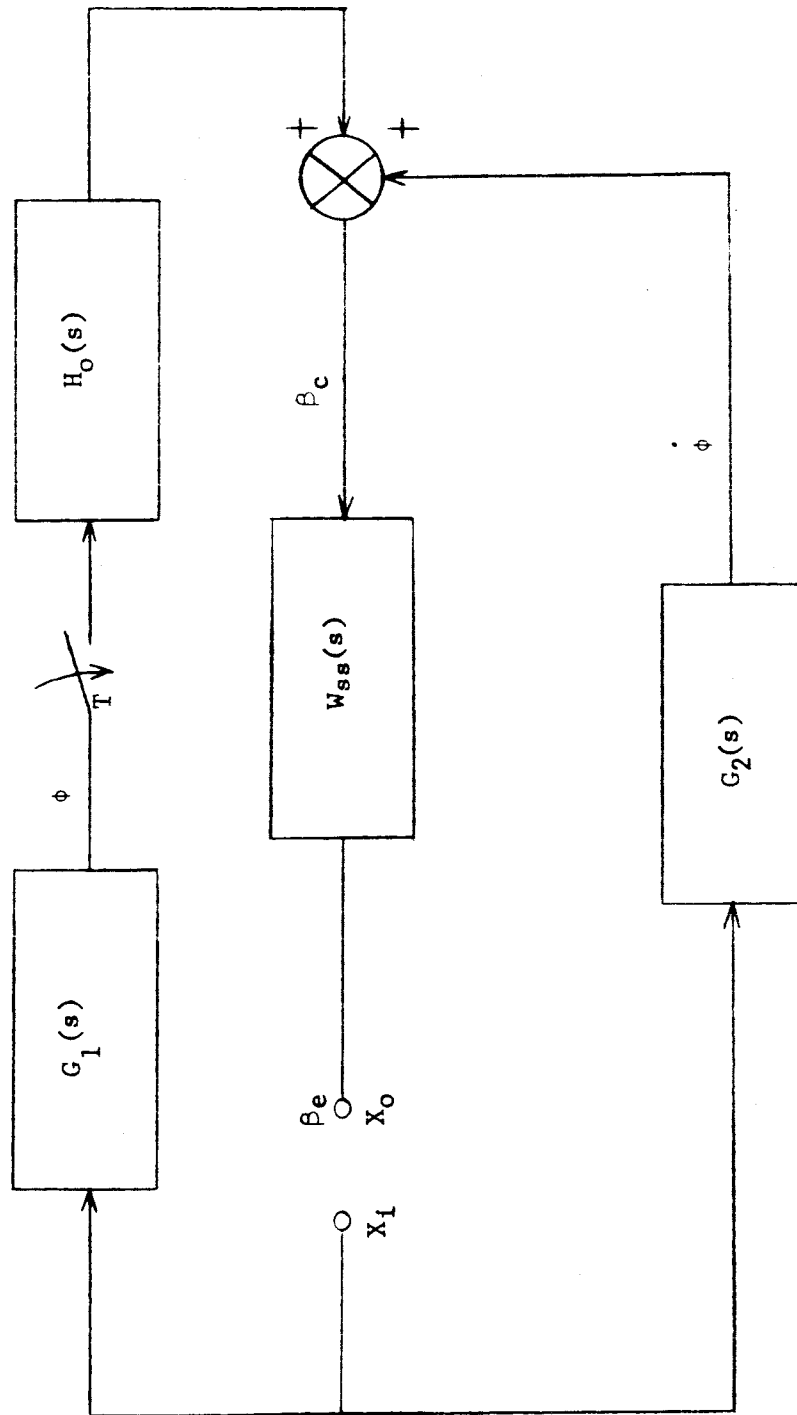


Fig. 2--System shown in figure 1 broken at  $\beta_e$ .

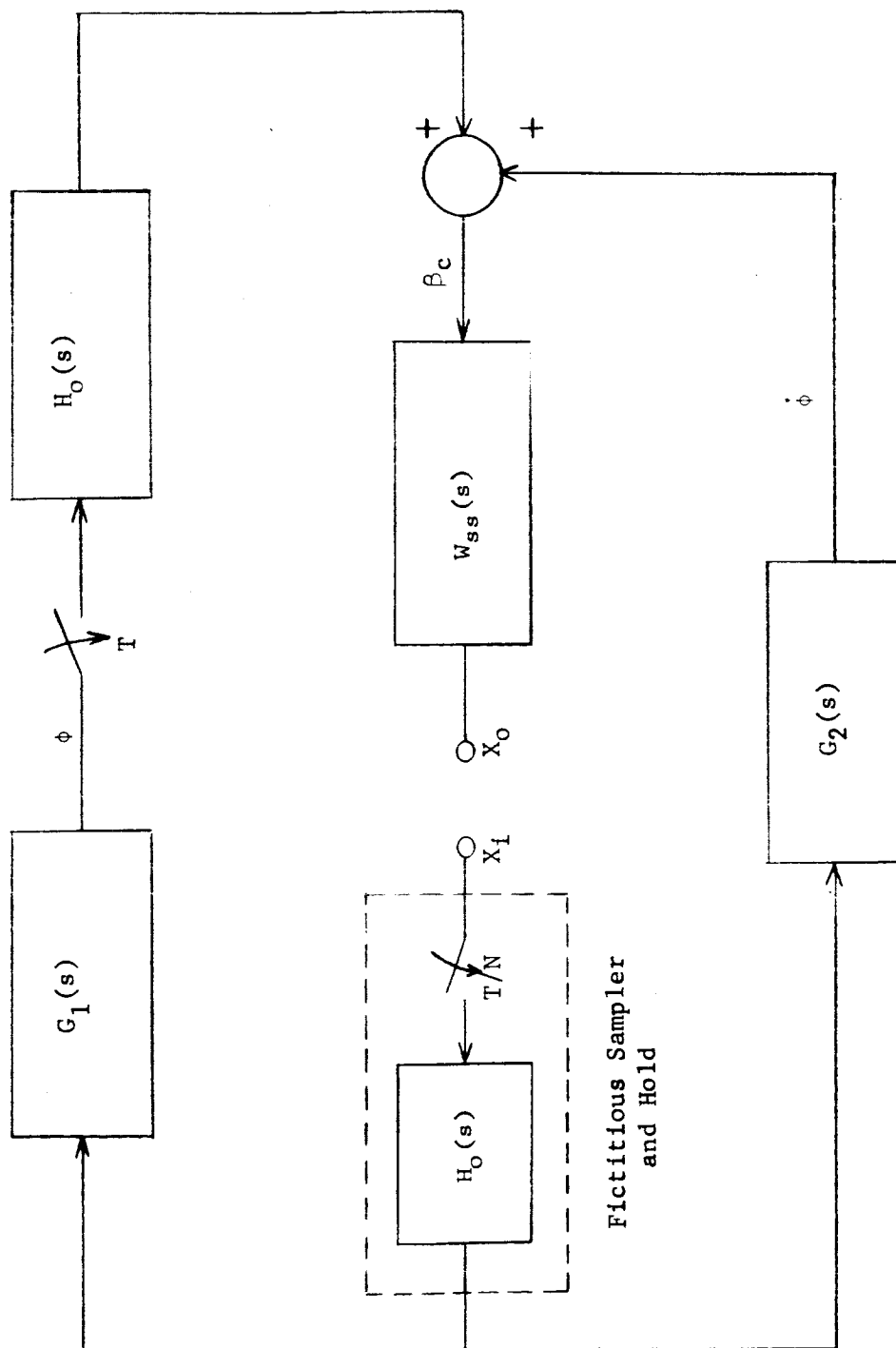


Fig. 3--System broken in  $\beta_c$  channel with fictitious multirate sampler and hold at input terminal

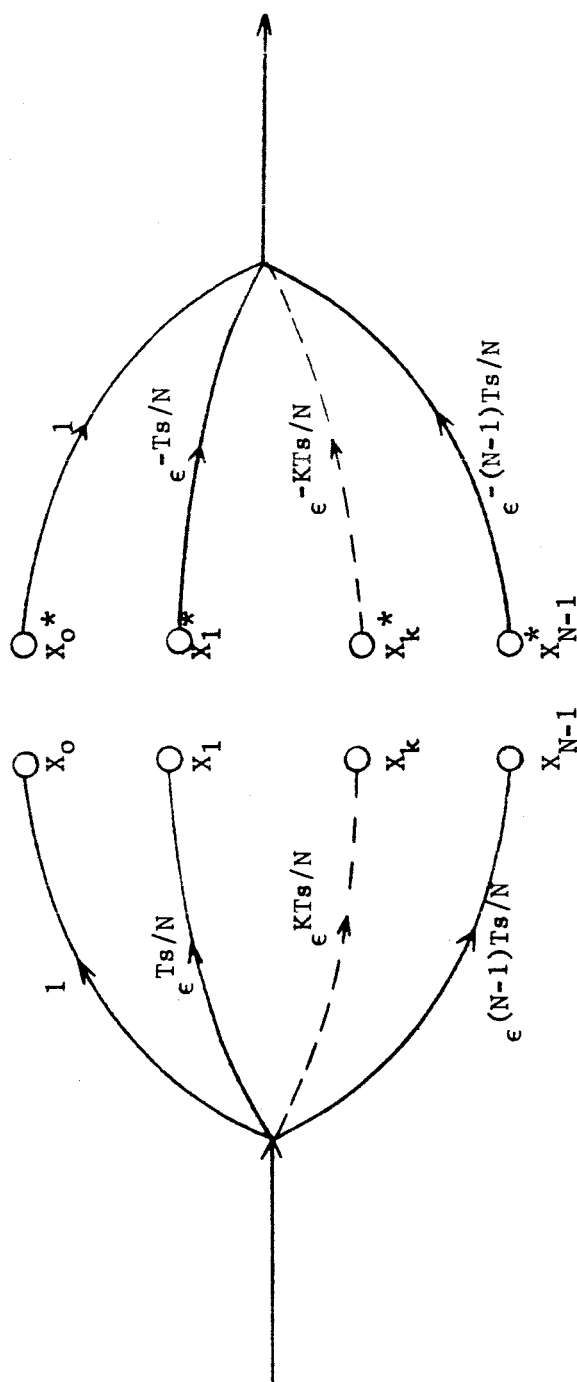


Fig. 4--Equivalent signal flow graph of multirate sampler

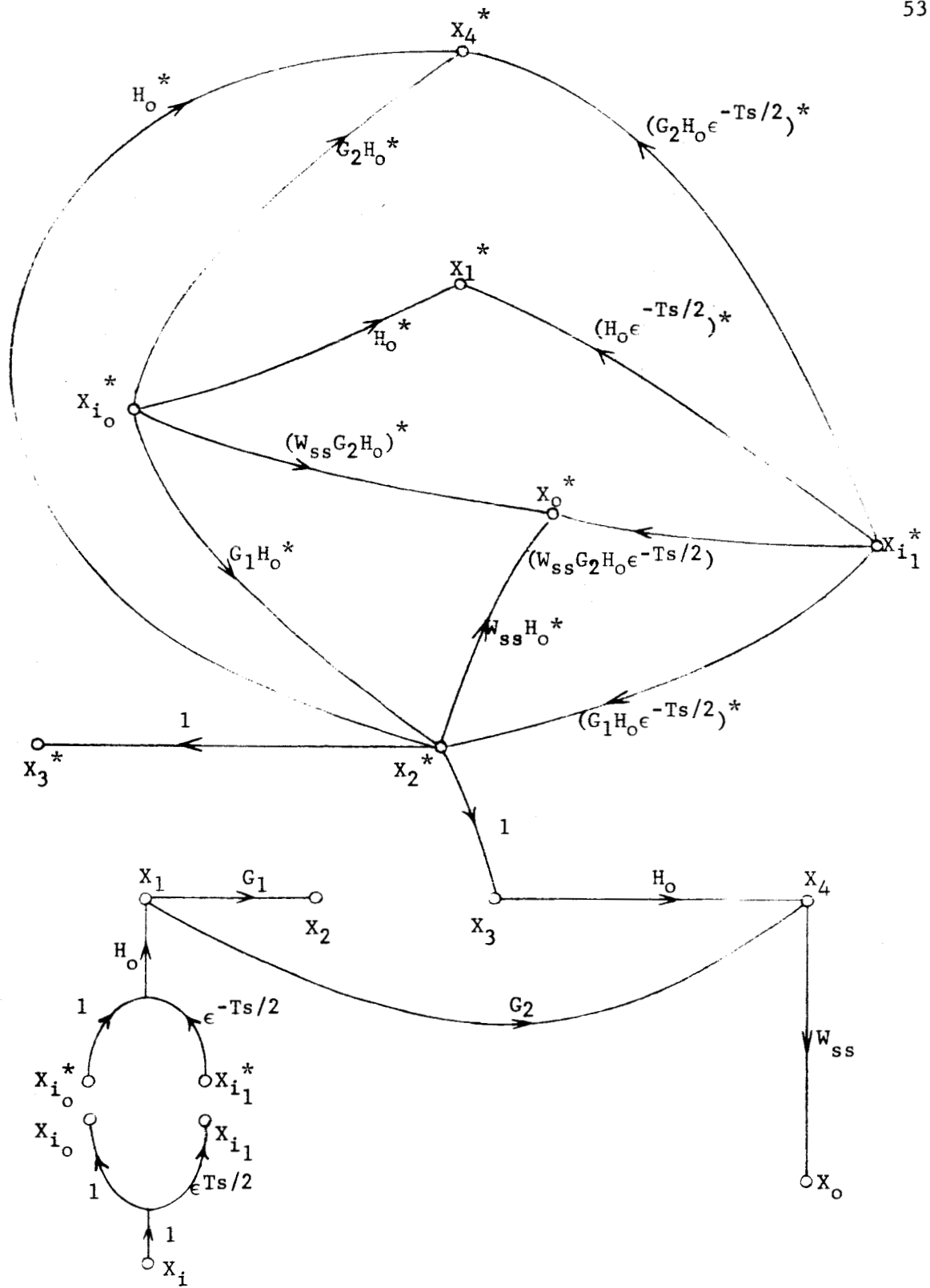


Fig. 5--Composite signal flow graph of figure 3 ( $N=2$ )

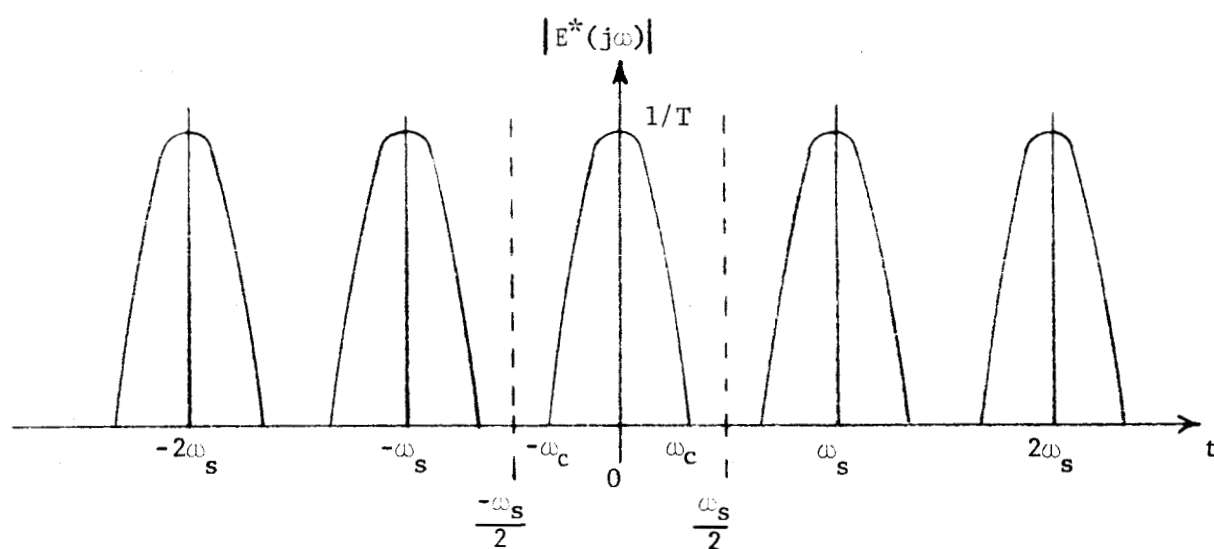


Fig. 6--Frequency spectrum of ideal sampler output



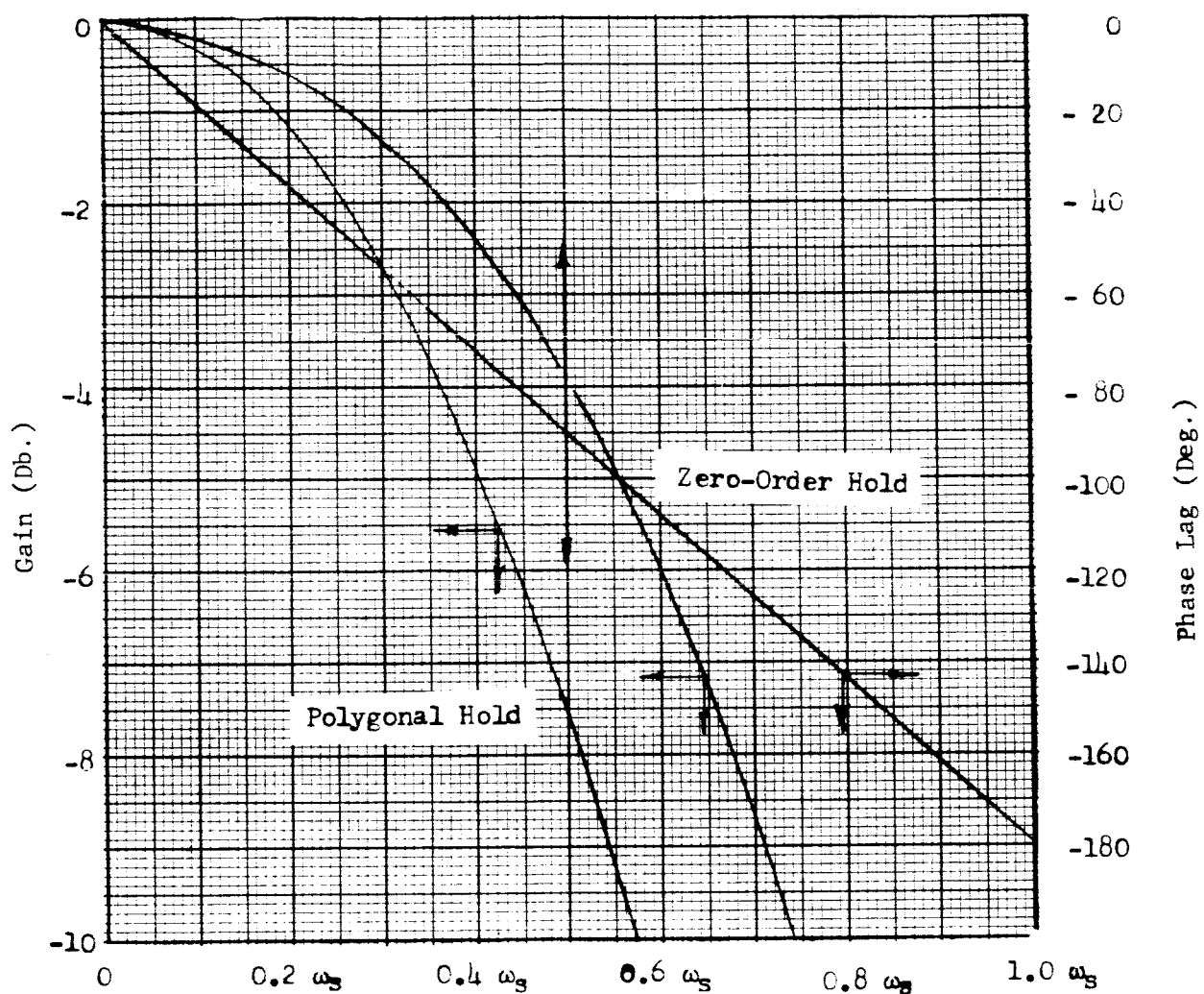


Fig. 7--Gain and phase response for zero-order and polygonal hold versus  $\omega$

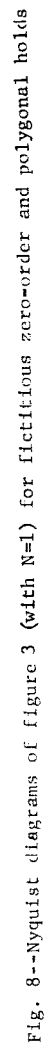


Fig. 8--Nyquist diagrams of figure 3 (with  $N=1$ ) for fictitious zero-order and polygonal holds

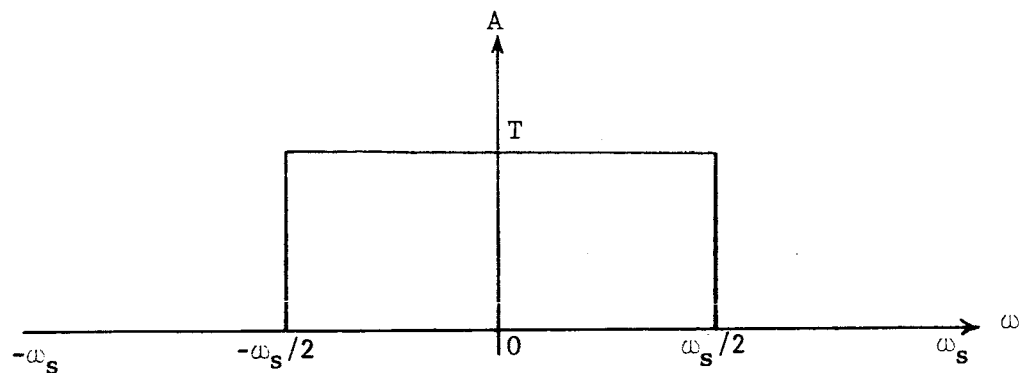


Fig. 9--Gain characteristics of ideal filter.

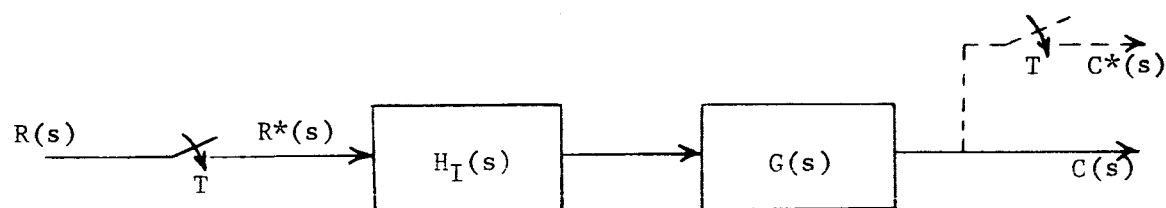


Fig. 10--Open-loop sampled system.

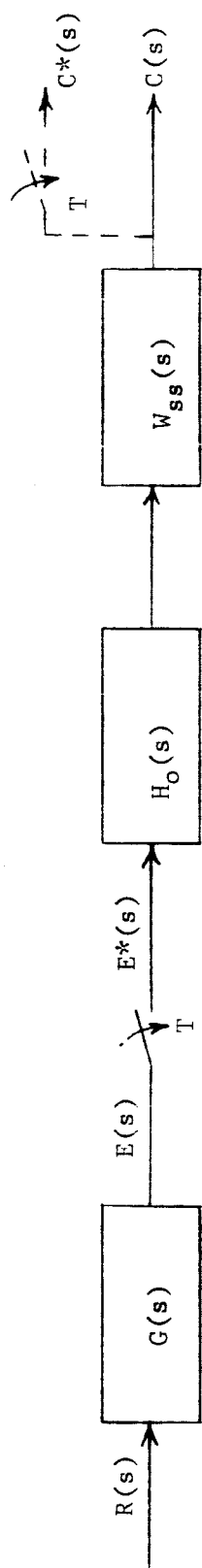


Fig. 11--Sampled system with an unsampled input.

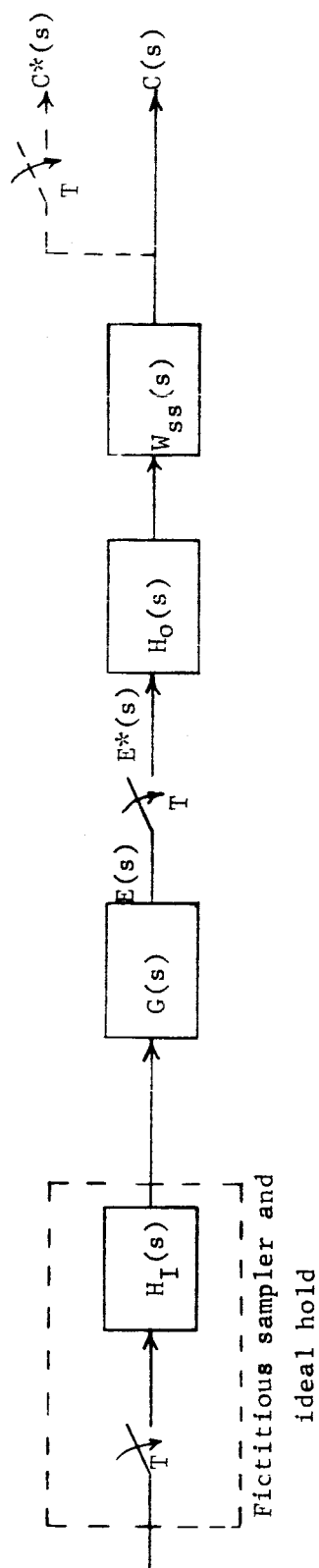


Fig. 12 --System shown in Figure 3 with fictitious sampler and ideal hold inserted at the input terminal.

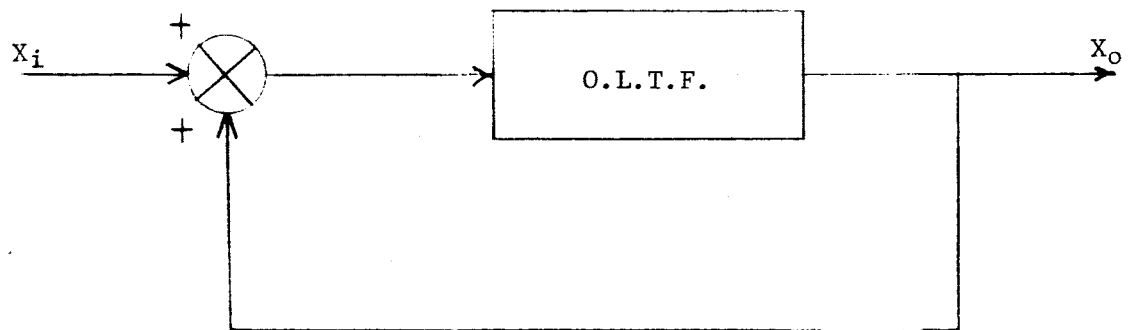


Fig. 13--System shown in figure 1 redrawn

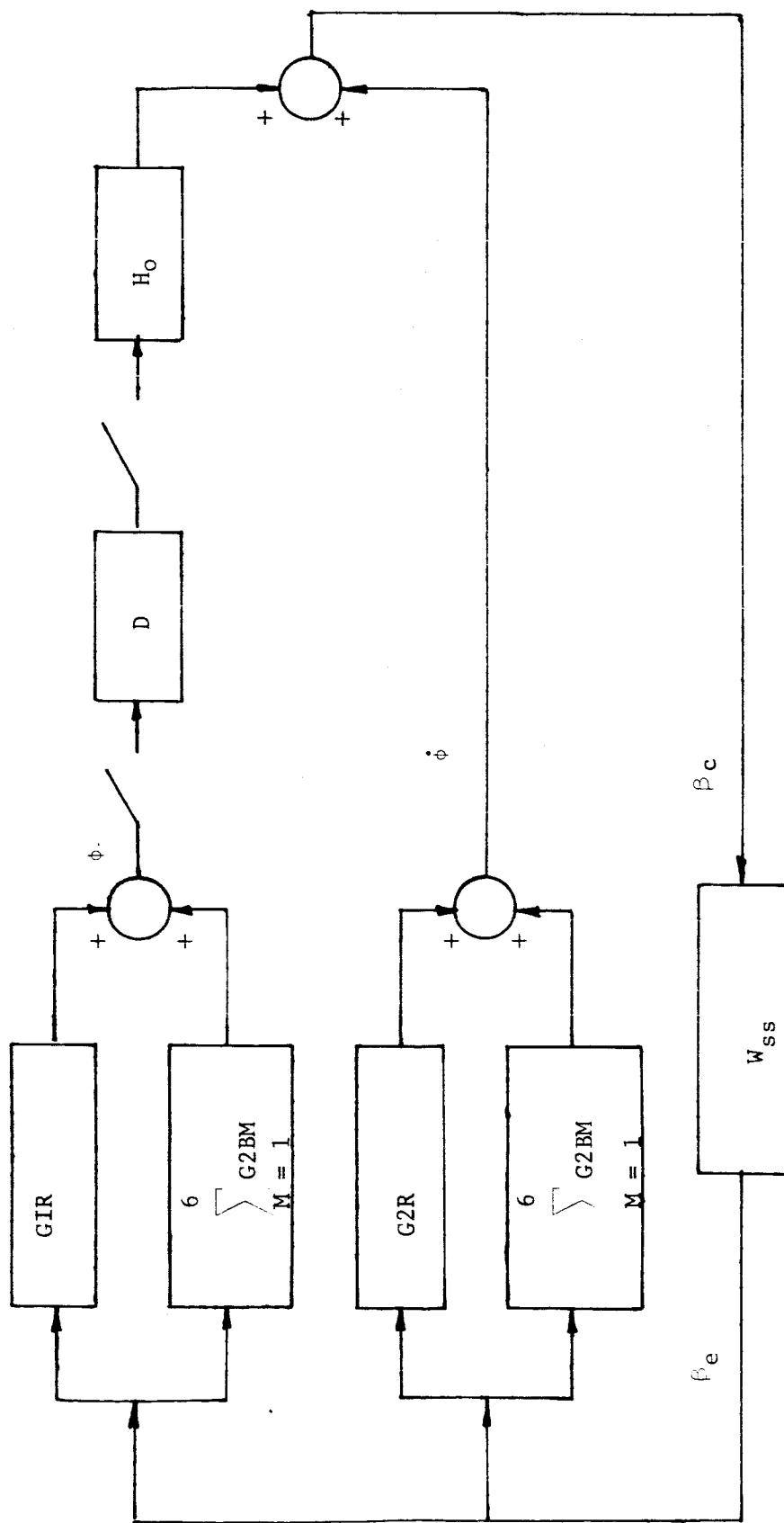


Fig. 14--Sampled system including bending modes

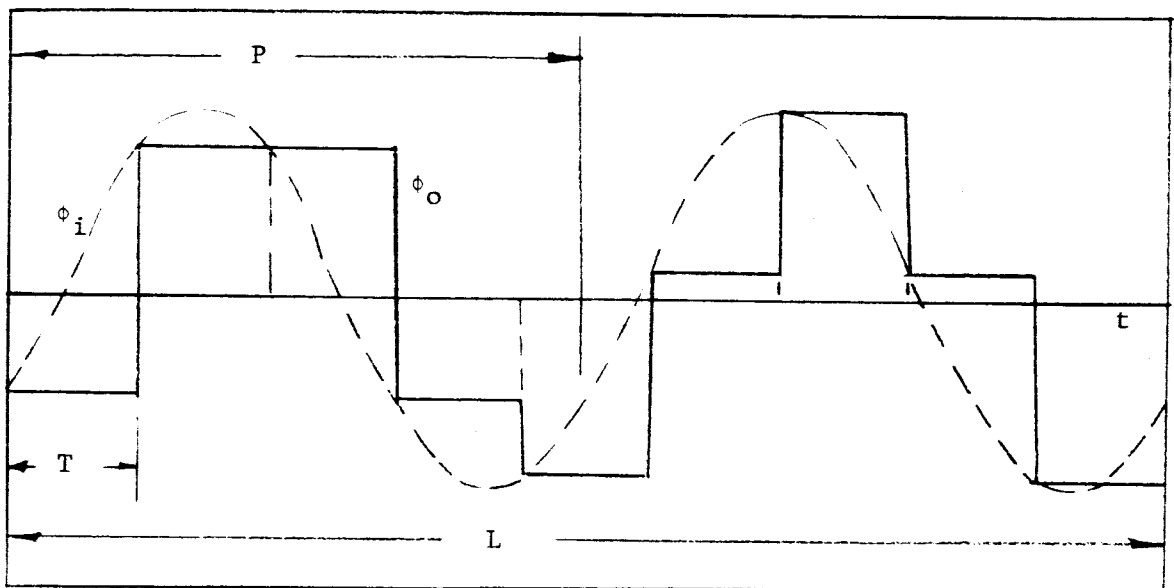


Fig. 15--Input and output wave of the sampler and zero-order hold

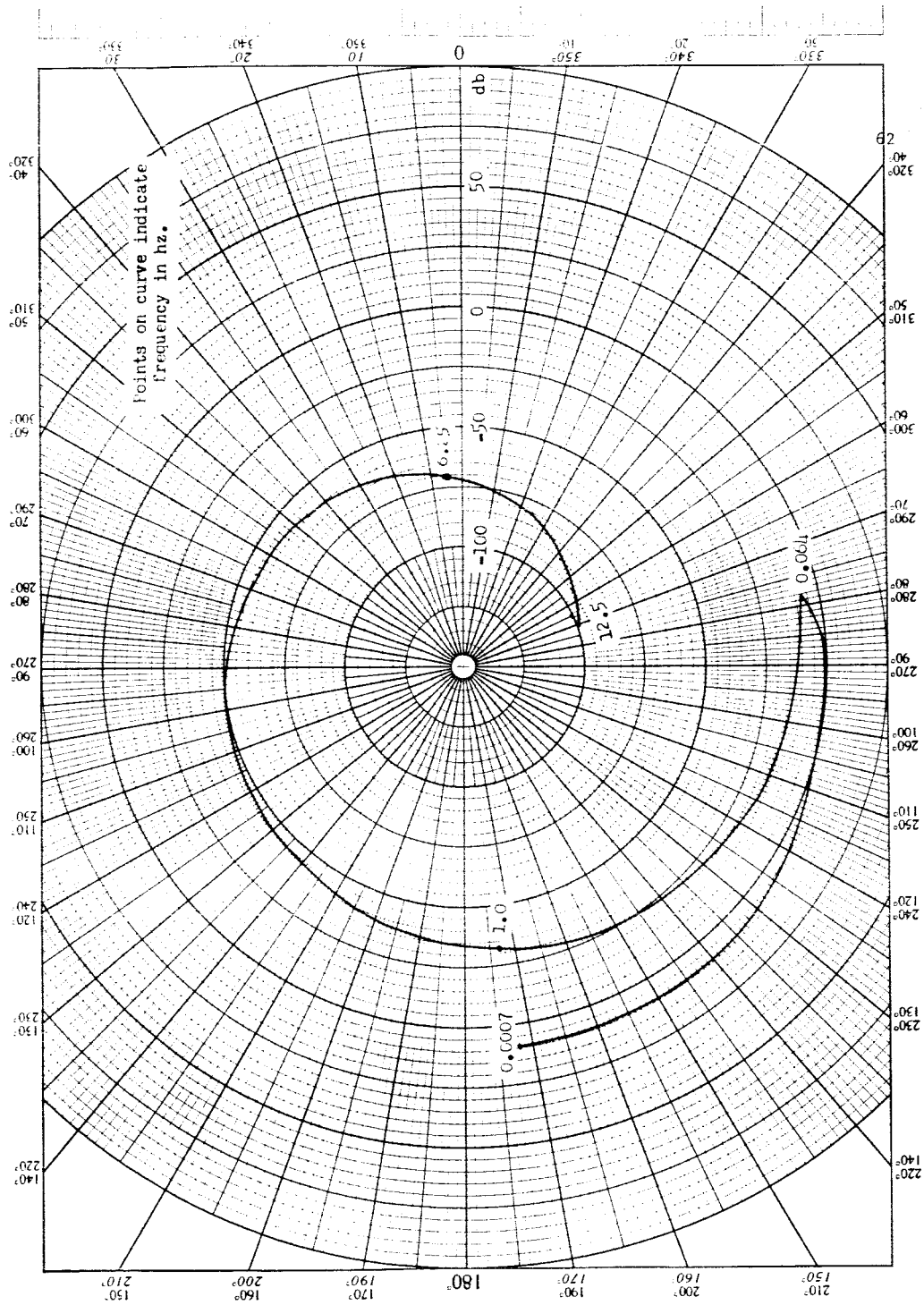


Fig. 16--Nyquist diagram for system shown in Fig. 14 opened in  $\phi$  channel (no bending modes)



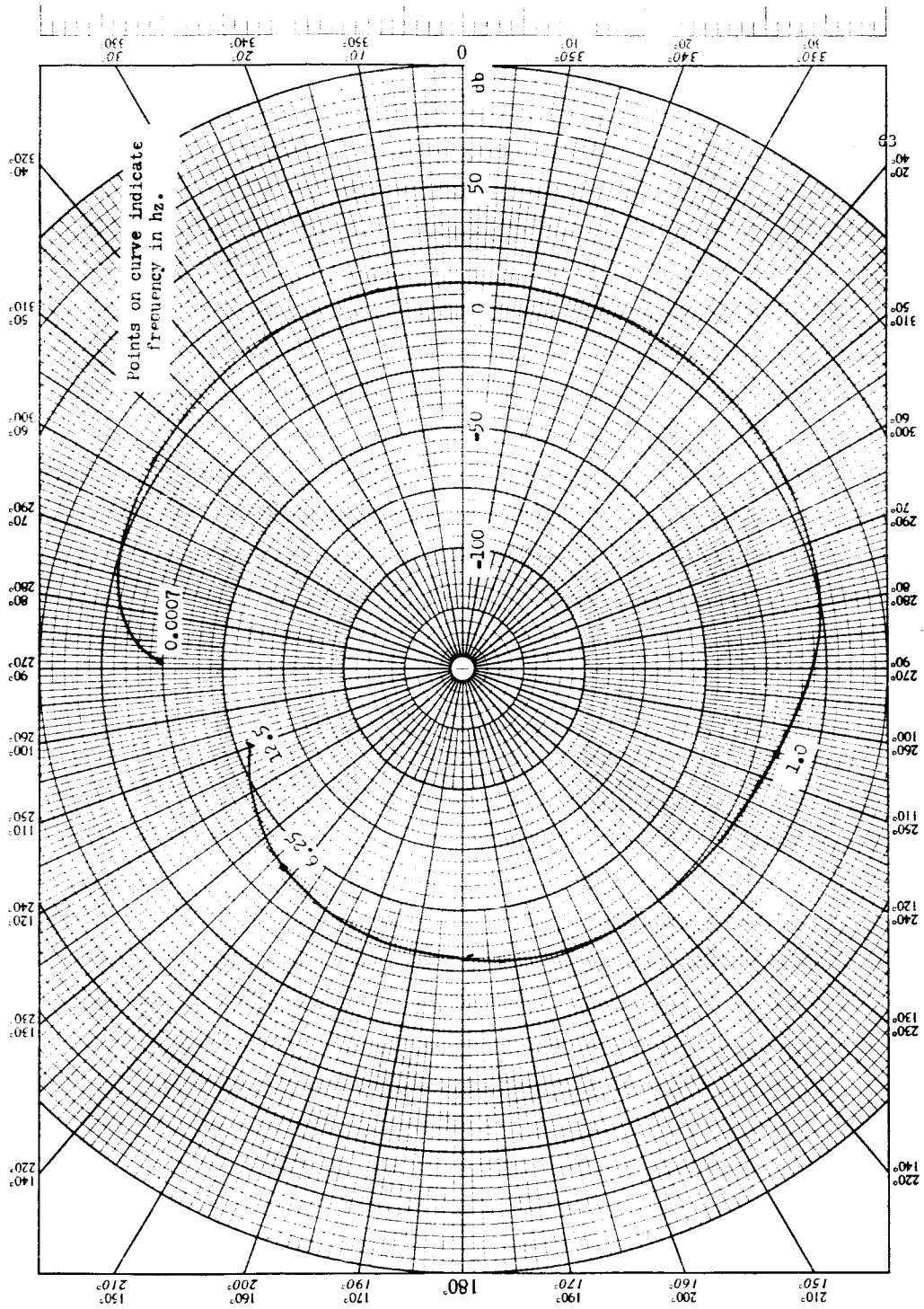


Fig. 17--Nyquist diagram for system shown in Fig. 14 opened in  $\phi$  channel  
(no bending modes)



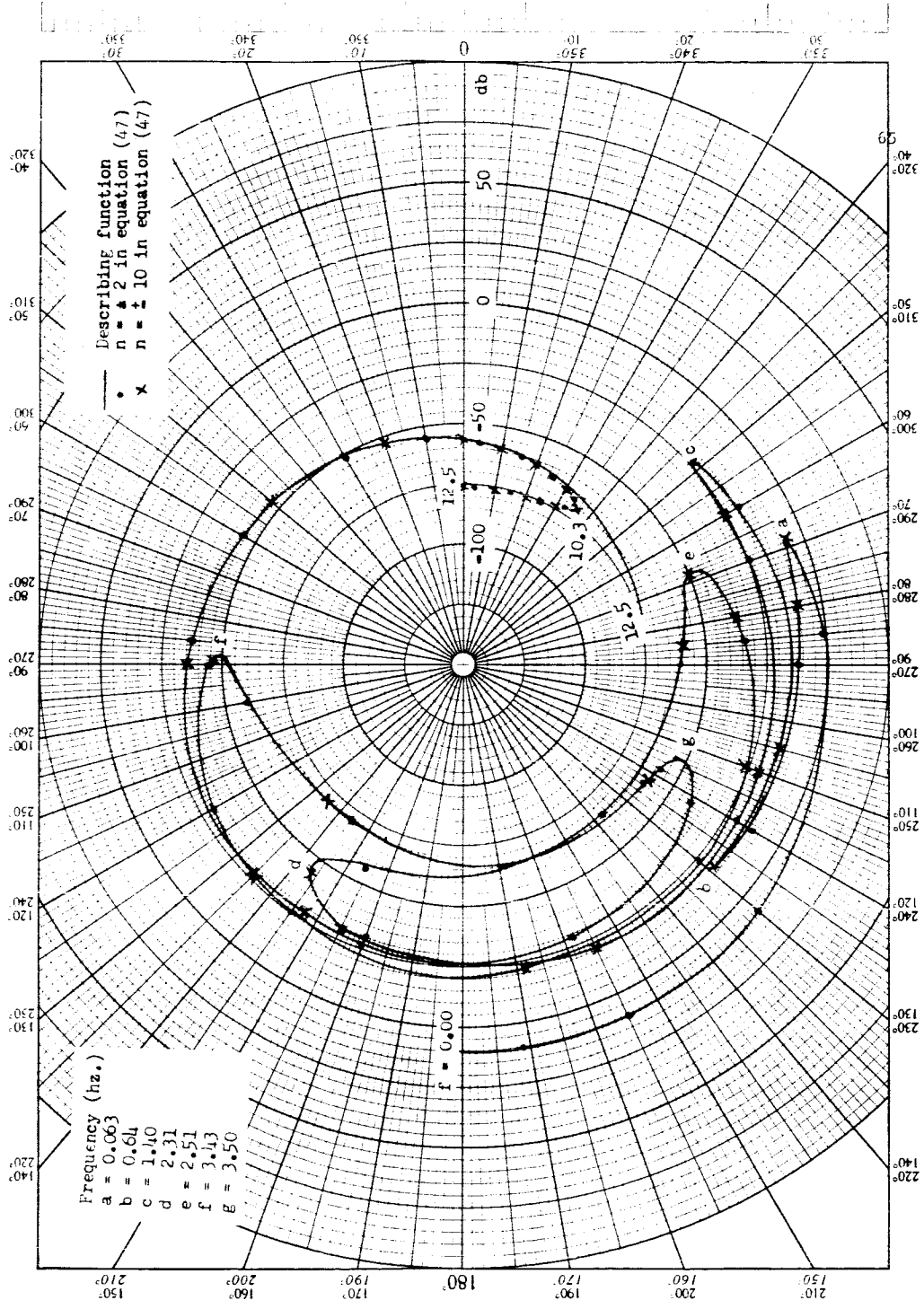


Fig. 19--Nyquist diagram for system shown in Fig. 14 opened in  $\phi$  channel  
(four bending modes)



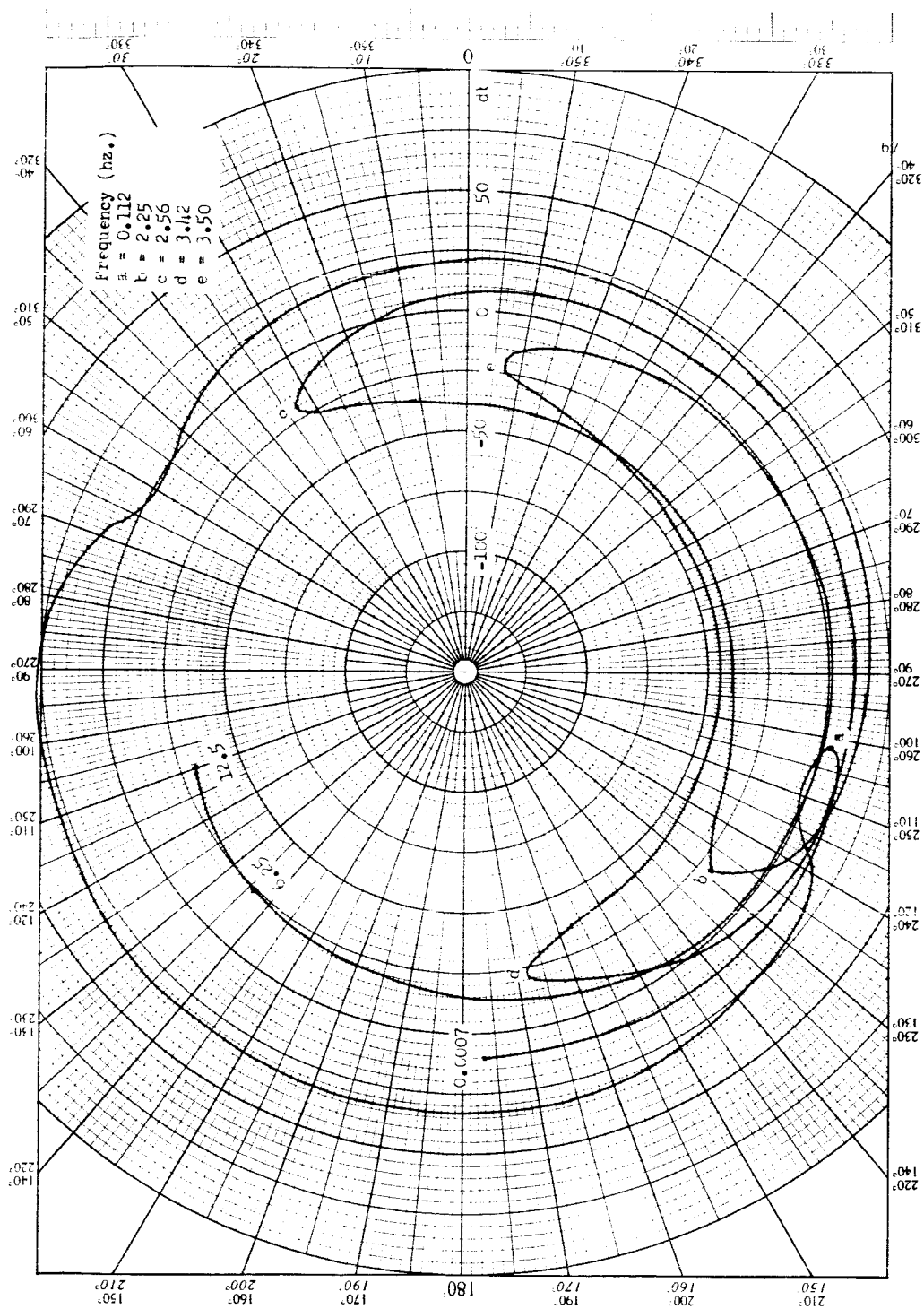


Fig. 21--Nyquist diagram for system shown in Fig. 14 opened in  $\bar{p}_c$  channel  
(four bending modes)

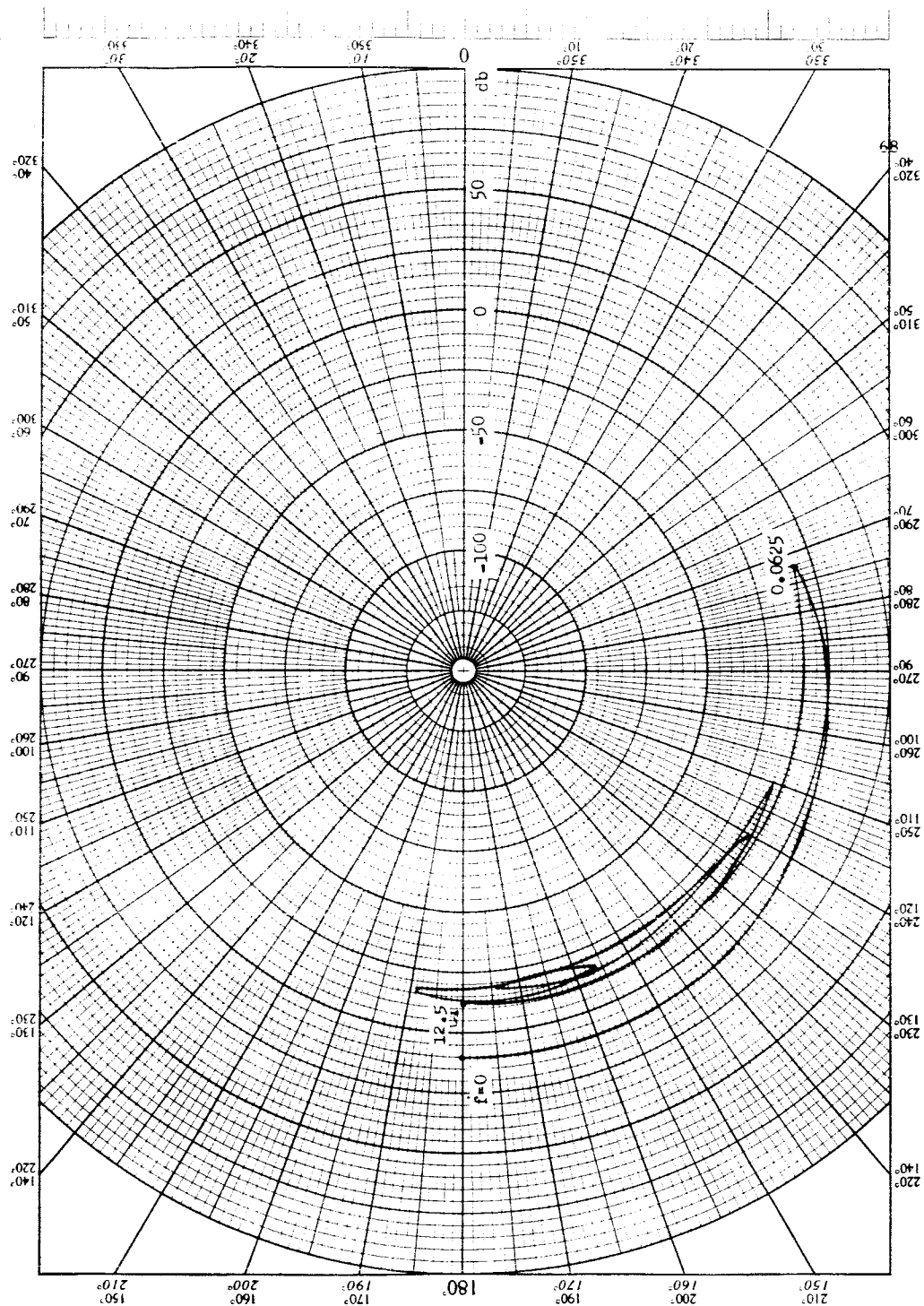


Fig. 22--Nyquist diagram for system shown in Fig. 14 opened in  $\phi$  channel using single precision Z-transform methods (four bending modes)